

---

# A behavioral setup for capturing fine grained coordinated movements of zebrafish larvae

Katharina Koetter<sup>1</sup> , Thomas Soares Mullen<sup>2</sup> , Younes Farouj<sup>1</sup> , Ot Prat<sup>1</sup> , Nathan van Beelen<sup>1</sup> , Michael Orger<sup>2</sup> , Ruben Portugues<sup>1,3,4,5</sup> 

<sup>1</sup> Institute of Neuroscience, Technical University of Munich, Germany

<sup>2</sup> Center for the Unknown, Champalimaud, Lisbon, Portugal

<sup>3</sup> SyNergy Excellence Cluster, Munich, Germany

<sup>4</sup> Bernstein Center for Computational Neuroscience, Munich, Germany

<sup>5</sup> Max Planck Fellow Group - Mechanisms of Cognition, MPI Psychiatry, Munich, Germany

contact: ruben.portugues@tum.de

date: January 2025

---

## Abstract

Animals use their whole body to navigate their environment and solve tasks. Identification of common dynamics of body parts using quantitative methods is key to study underlying motor system organization. Zebrafish (*Danio rerio*) need to coordinate tail and pectoral fin movements and can serve as a model organism for the study of locomotion generation. Behavioral tracking of larval zebrafish has usually restricted itself either to track only the position and tail movements of freely swimming zebrafish larvae, or to track fine movements of body parts in immobilized fish. This precludes studies that investigate coordination or postural control.

To study full body coordination, we built a setup that allows us to track freely swimming larval zebrafish, while acquiring high resolution images of their whole body. This enables tracking of both tail and fins using DeepLabCut with additional segmentation and classification of the tail using the Megabouts algorithm. First, we describe stereotypical fin dynamics at bout onset which show differences between modes of movements as forward swims and turns. Thereafter we show that fin dynamics can be embedded on a low dimensional manifold with axes corresponding to amplitude, vigor and frequency. Based on this embedding, fin dynamics show a degree of stereotypy with associated tail classification. Lastly, we show that a model that captures the latent dynamics underlying tail movement generation, developed using ILQR-VAE, is able to predict fin dynamics, hinting towards a coupled control mechanism. Overall, this represents an important step towards building a comprehensive dictionary of larval ze-

brafish locomotion that will enable better study of motion generation and coordination.

## Introduction

In recent years, interest in naturalistic behavior among physiologists has grown into the field of computational neuroethology [1], which studies brain activity during unrestrained and ecologically-relevant behaviors aided by modern computer vision tools [2]. Historically, neurophysiology setups required restraint of the animal and used task-based experimental paradigms, such as conditioning paradigms. In such conditions, the richness and complexity of behavior that animals exhibit in the wild may not be adequately captured [3–5]. Nevertheless, even in such constrained tasks, subtle movements can have a large effect on neural dynamics [6, 7]. Modern approaches allow for recording both brain activity and enable freely behaving animals, providing a holistic and unbiased observation of behavior necessary to properly interpret neural activity data. Several studies have already made steps towards a more holistic understanding of the animal's interaction with its environment in *C. elegans* [8, 9], larval zebrafish [10–13] and mice [14]. The full and unbiased observation of behavior is especially important to study of motor coordination, which benefits from observing animals during complex interactions with their environment.

Technical progress in methods and data processing has accelerated the possibilities in this research area. We have seen advances towards more portable high speed and high resolution imaging methods, fast deep learning-based unbiased annotation and segmentation algorithms [15–17] and a lower cost in cloud computing necessary for data processing.

Together with improved tracking, the need for behavioral segmentation and classification algorithms that can deal with complex data in an automated manner has arisen. Previously, segmentation and labeling of behavior was performed manually, which was an intensive task prone to bias. It also depended highly on knowledgeable experimenters and good domain knowledge, thus limiting throughput. Recently more software has started to emerge based on researchers needs. From the automatic classification of tail movements in zebrafish to pre-existing categories [18] to software that segments video data into reoccurring behavior syllables, e.g. in mice (MoSeq [16, 17] and zebrafish [19, 20].

While the segmentation of behavior in many species is challenging due to its continuous nature, the behavior of larval zebrafish (*Dario rerio*) is naturally segmented into discretized movements called 'bouts'. Larval zebrafish swim in a burst and glide fashion alternating with regular inter bout intervals. Through an extensive study of stimuli and context, the behavioral repertoire of the tail is stereotyped and can be mapped into 13 bout categories [21] using software Megabouts [18]. The tail itself is an alternating sequence of left and right tail bends that can be modulated in various ways, e.g. in the ballistic period [22], for the fish to have fine grained control over the behavioral variables of each movement, such as speed and direction. This makes zebrafish an good model organism to study the effect of coordination between body parts with respect to the behavioral output and modulation of parameters of the movement.

For the study of coordination and generation of movement all body parts need to be taken into account to facilitate understanding, as animals frequently couple bodyparts dynamics to facilitate efficient locomotion. In the case of larval zebrafish, they coordinate two anterior bodyparts (pectoral fins) and a posterior bodypart (tail) to produce stable and efficient swims, yet fins are hard to image due to their small size. One of the earliest studies to look at fin movement has described the fins oscillatory dynamics [23] in slow swims. By capturing single spontaneous swims under a high-speed camera they have shown that when a movement is initiated one fin is leading ('leading fin') while the other ('trailing fin') oscillates jointly with the tail where the speed of the fins are correlated. This indicated that the fin dynamics are coupled to tail dynamics in a coordinated way, exemplifying the whole-body coordination. However, this study only taken into account one bout category, so it is still unclear which role fins play for other types of movement. Other studies have started to describe fin movements for other bout categories, such as escapes in particular, where they found no to little fin involvement, whereas some turns, e.g. J Turns, tend have highly variable fin dynamics [24]. Fins therefore have rich dynamics that are associated with tail movement to fulfill different functions during locomotion.

Morphologically the fin is composed of a flexible endoskeletal disk [25], a fin membrane with spear-like collagen complexes and two muscles that innervate the disk along the sagital plane [26]. Candidate Central Pattern Generator (CPG) neurons for a potential circuit could be traced back from abductor-adductor motor neurons innervating the muscles to the spinal cord [27]. These motor neurons control fin movements by a push-pull mech-

anism and underlie upstream control through *dmrt3a*+ commissary interneurons in the spinal cord [27]. Experiments in larval zebrafish have suggested that rhythm generation of the tail is organized in a modular way and distributed onto two sets of morphologically and molecularly different neurons (VO and V2a) that activate at different locomotion speeds [28–30]. Fin behavior has been shown to be gaited to locomotion speeds in juvenile reef fish [31], however, how fin and tail dynamics are generated on a neuronal level remains unknown.

Even though some behaviors such as Short Latency C-Starts can be trigger by the activity of a single neuron (the Mauthner cell) [32], recent modeling suggests that tail movements for all bout categories can be generated by a shared latent network that differs on initialization parameters [33]. The complete fin abduction-adduction cycle was similar to the duration of the tail cycle, indicating a shared coupled or nested network [26]. In order to investigate coordination and motor pattern generation, we must describe fin dynamics and their interplay with the tail during naturalistic behaviors in detail.

Since earlier studies had a limited number of movements and were based on manual annotation, we need a more extensive dataset that captures different types of movements. For this we built a tracking setup that allows continuous fin and whole body imaging at high resolution and acquired an extensive data set of more than 10000 movements that capture spontaneous zebrafish behavior. We trained a DeepLabCut network for reliable key point annotation to extract data in an automated manner and automatically segmented as well as classified the tail with Megabouts [18] to avoid manual classification bias.

First, we found stereotyped movement onset dynamics of fins that deviate for forward movements and turns. Next, we described the features necessary to generate the spectrum of fin dynamics by embedding fin dynamics onto a low dimensional manifold that varied along amplitude, frequency and a non-linear time frequency relationship. Some, but not all, bouts that shared tail dynamics also shared similar fin dynamics leading to a measure of stereotypy proposed for fin movements.

Therefore we investigated, whether tail and fin dynamics could be generated by the same underlying network. For this we employed an iLQR-VAE network, trained to learn a sparse representation of tail dynamics [33]. The network was blind to fin dynamics but was nevertheless able to predict fin traces. The prediction accuracy depended on fin features described earlier with fins with lower number of oscillations and amplitude being more difficult to predict.

## Results

### High spatial resolution acquisition of behavior of zebrafish larvae

In order to image fins in freely swimming zebrafish larvae at high resolution, we built a setup that tracks the fish swimming in the experimental arena (Figure 1A) utilizing a 3 axis motor system with a 20 cm travel range in the XY axis and 7 mm in the Z axis (see Methods 0.0.1). This dramatically increased our resolution and enabled

us to image the fins. To avoid motion blur we imaged at 200 fps using a high power infrared illumination box. The open source software Stytra was extended with an on-line tracking loop that included a fish detection pipeline operating with a sub-millisecond performance [34].

64 WT pigmented fish aged 6-7 days post fertilization (dpf) were tracked while swimming spontaneously in an arena for the duration of the experiment (10 minutes). Four example trajectories can be found in Figure S1A. We trained a DeepLabCut model on our videos to annotate 14 key points along the fish body (see Methods 0.0.1, Figure 1B). We extracted abduction angles for fin and tail and cropped into segments lasting 250 ms, each corresponding to a single bout (shaded regions in Figure 1C).

We assessed the quality of our tracking by quantifying the tracking error as distance from the mid-head key-point to the center of the image (Figure S1B). For 99% of frames the tracking error was below 2 mm for all bouts (Figure S1C), while faster bout types having larger tracking errors as expected due to the lag in motor initiation when the fish accelerates rapidly (Figure S1D).

To estimate the duration of the fish being tracked, we quantified the number of frames where the body key-point had a likelihood above 0.95 in DeepLabCut. In 61% of all experiments conducted, 90% of frames were had the fish tracked successfully (Figure S1E). In order to assess the quality of our fin key-point annotation, we quantified the percentage of frames where all fin points were annotated with 0.95 or above likelihood (Figure S1F). We observe that the fins are annotated well within 80% of frames with the fish tracked.

To assess the tracking performance of our setup, we looked at the duration of episodes when the fish was tracked. The duration of episodes showed a bimodal distribution (Figure S1H). This indicates that the fish is either lost frequently or tracked reliably for the entire duration of the experiment. When a tracking failure occurred, the search algorithm (see Methods 0.0.1) recovered the fishes position in under a minute in 68% of cases (Figure S1G).

We start by describing an example of fins during a *Burst Swim* (Figure 1C-E, more Examples in Figure S3). At bout onset, both fins are abducted before changing the pattern from synchronous initiation to alternating coordination after the first fin beat. The fins show the expected pattern of alternating oscillations before returning to the side of the body at rest. For the example bout, we observed a longer fin beat period of the right fin, a different number of oscillations between the fins and a varying amplitude of abduction peaks.

For a comprehensive description of tail movement we used the recently published pipeline Megabouts [18] to classify extracted bouts (Figure 1F). The distribution of bout categories aligns with the expected fish behavior during spontaneous swimming, as observed in previous studies [18, 21]. These studies reported that during spontaneous swimming under a light background a large proportion of bouts are *Slow1* and *Slow2*, as well as *Routine Turn*, *High Angle Turn* with decreasing probability. We cannot rule out potential influences of the setup and environment on their behavior as we observed a small number of typical escape behaviors (*SAT*, *Obend*, *LLC*, and *SLC*), indicating that some fish might be experiencing stress due to the movements of the motor.

To assess the fish behavior in our setup, we investigated behavior metrics including body angle, fin angles, bout distance and inter-bout interval for an example fish (Figure S2A-C) as well as for all fish (Figure S2D). The bout angles show the expected trimodal distribution (Figure S2D). Fins can move in range from 0 to 100 degrees with negative angles for left fins and positive angles for right fins (Figure S2D). The mean bout distance was  $0.77 \text{ mm} \pm 0.98 \text{ mm}$  and the mean inter-bout interval  $1.52 \text{ mm} \pm 3.91 \text{ mm}$  (Figure S2D, bottom row), which are slightly lower than in other freely swimming setups. We concluded that our fish exhibited a natural range of freely swimming behavior in our setup and continued to describe more detailed fin dynamics.

## Characterization of fin dynamics during bout onset reveals Stereotyped dynamics

Previous studies have described fin dynamics as a series of alternating rhythmic movements started after asymmetric first fin abduction, with the first fin to complete abduction is classically defined as 'leading fin' and the other as 'trailing fin' [23]. The fins are usually anti-correlated with each other [23]. Common characteristics of the leading fin included lower amplitude, higher velocity and shorter fin beat duration [23]. However, this description was based on a small number of observations from limited bout categories, therefore we wanted to expand upon previously described dynamics using our data set and a naming system of ipsilateral (same side as first tail undulation) and contralateral (opposite side to first tail undulation) fin (Figure 2A-B).

At first glance, ipsi- and contralateral fin show different coordination between two modes of movement (forward swims and turns) such as difference in amplitude of first fin abduction (Figure 2C). The 'leading fin' is predominantly the ipsilateral fin for turns (Figure 2D), e.g. when the fish is turning left, the left fin initiates the movement. For forward swims, such as *Approach Swim*, *Slow 1* and *Slow 2*, fish do also use the contralateral fin for a number of initiations.

Other studies already described a bias in first head movement or tail undulation [35] as well as motor asymmetry mediated by neurons in the Posterior Tuberculum [36]. Therefore we assessed if fish have a bias in their preferred leading fin to initiate forward bouts primarily as turns are more stereotyped in choice of leading fin. We calculated a laterality index based on the ratio of left vs right fin usage (see Methods 0.0.3, Figure S5A). We can observe that 48% of fish do not have a clear preference, while other fish above or below the quantile were classified as having preference (quantile range: -0.13 to 0.12, Figure S5B). The leading fin preference did not bias the bout angle in forward bouts (Figure S5C). This indicates a whole circuit bias for movement initiation.

In a small fraction of bouts, we were unable to accurately identify the leading fin and thus included leading fins with less than 5 ms difference as having 'Equal' leading fins, as described before in [23] (Figure 2D). We observe an increased fraction of 'Equal' leading fins in escape bout categories (Figure S4A) in line with previous descriptions of e.g. 'tuck' fin movement patterns [37]

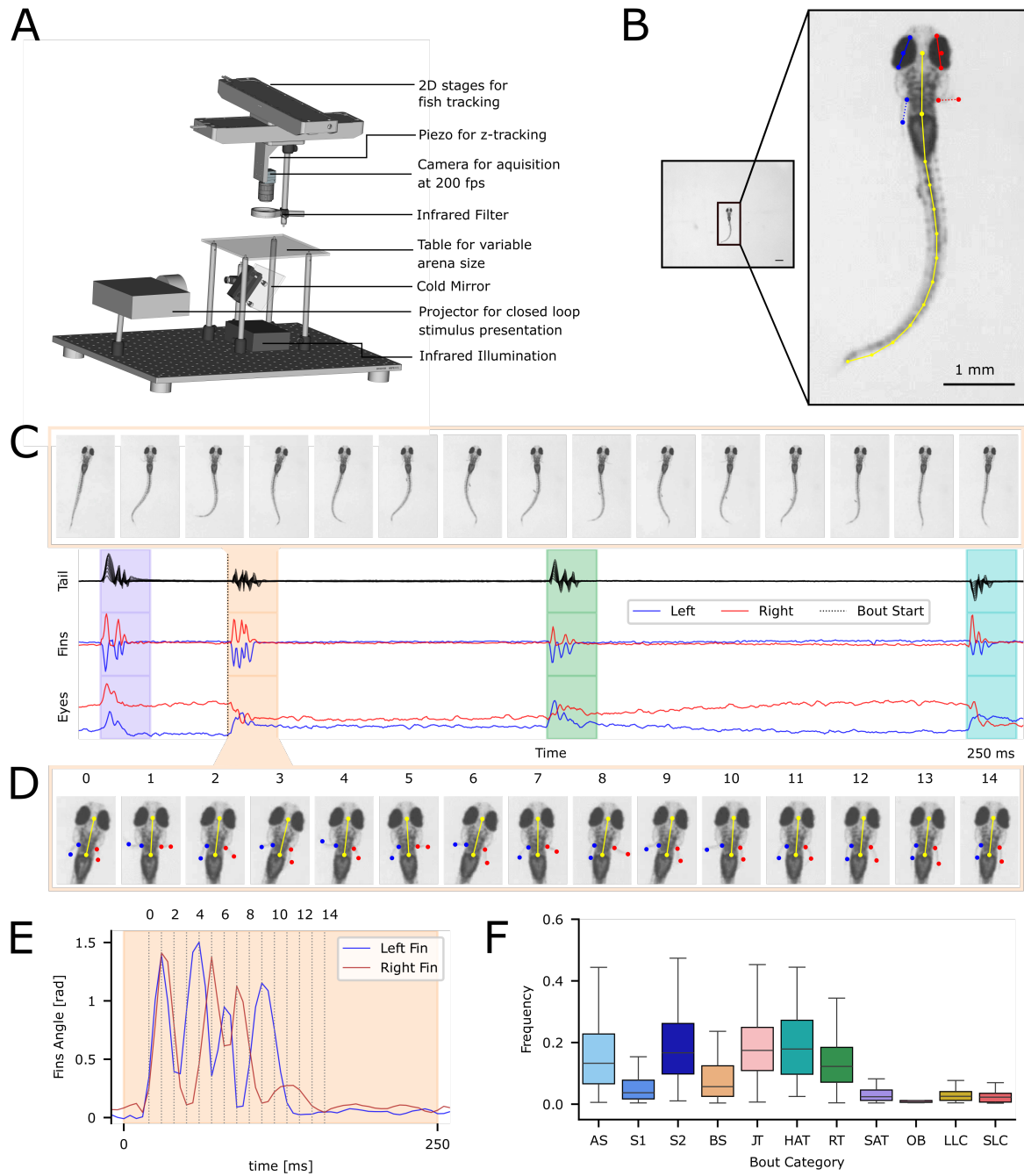


**Figure 1: High spatial resolution acquisition of behavior of zebrafish larvae.** (a) Schematic of Tracking setup as detailed in Method 0.0.1, (b) Reference frame of fish (left) with sub-panel (right) of fish with annotated DeepLab-Cut key-points as described in 0.0.1, (c) (top) Selected frames of fish during *Burst Swim* (peach). (bottom) Tail angle for a selected time window during the experiment. Background of extracted swims are shaded according to bout category based on Megabouts [18]. Left (blue)/right (red) Fin and Eye angle shown below for each swim. (d) Selected frames from *Burst Swim* annotated with mid head and body key-points (yellow) as well as left (blue) and right (red) fin key-points, (e) Fin angle during *Burst Swim*. Left fin (blue) flipped for better comparison. Timestamps of selected frames from (d) are annotated throughout the bout with dotted line, (f) Frequency of bout categories for the entire data set (normalized).

and fin movements during escapes [24].

To further investigate the timing of the body parts during bout onset further, we plotted the bout-triggered av-

erage of the three body parts up to 45 ms. We observed that the timing of movement between the body parts follows a pattern (Figure 2E, top). The ipsilateral fin initiates,



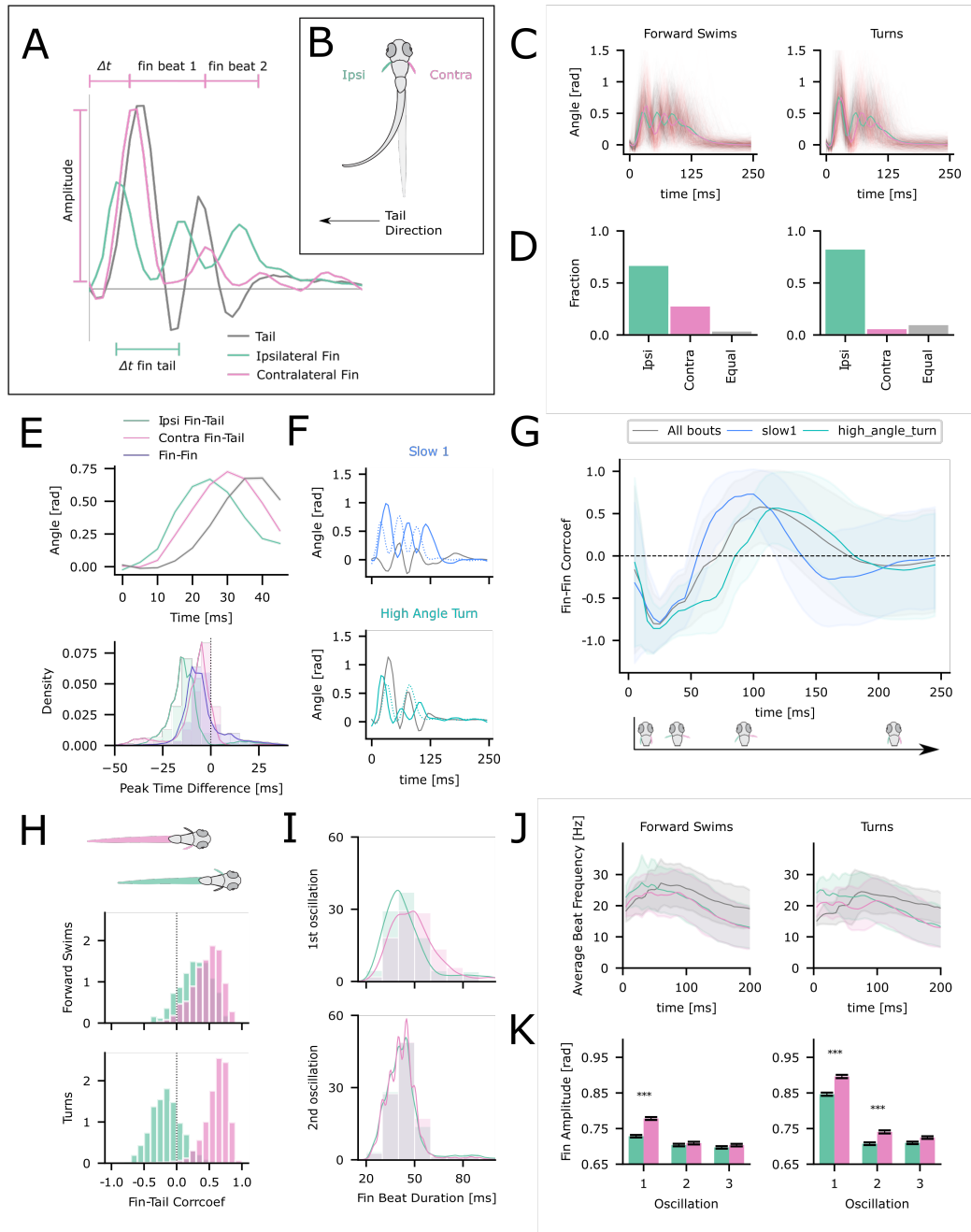


**Figure 2: Characterization of fin dynamics during bout onset reveals stereotyped dynamics.** (a) Example tail and fin angles with annotated features quantified in the analysis including Fin Amplitude, time to onset of bodypart ( $\Delta t$ ), timing differences between fin and tail ( $\Delta t$  fin-tail) and duration of fin beats, (b) Schematic of fish with annotated Ipsi- and Contra-lateral Fin based on Tail direction, (c) Example traces (n=500) of Ipsi- and Contra-lateral fin plotted for forward bouts and turns with mean trace per fin, (d) Histogram of leading fin for forward swims and turns, (e) (top) Bout triggered averages up to 45 ms, Mean with Standard Error or the Mean (SEM), (bottom)  $\Delta t$  between Ipsi- or Contra-lateral Fin and tail as well as between Ipsi- and Contra-lateral Fin (slate-blue), (f) Example Fins for a Forward Swim (slow1) and a Turn (HAT), (g) (top) Fin-Fin Correlation during the bout for example forward swim (slow1) and example turn (HAT) as well as for all bouts. (bottom) Schematic of fin movements during bout, (h) Correlation of Ipsi- or Contra-lateral Fin and Tail, (i) Fin Beat duration for two consecutive oscillations of Ipsi- and Contra-lateral fin, (j) Instantaneous Tail Beat Frequency (TBF) and instantaneous Fin Beat Frequency (FBF) for Ipsi- and Contra-lateral fins for forward swims and turns plotted as mean line with SEM, (k) Fin Amplitudes of Ipsi- and Contra-lateral fin for consecutive fin oscillation cycles for turns and forward swims.

while contralateral fin and tail follow with a varying timing in abduction across movement categories (Figure S4B). The ipsi- and contralateral fin on average precedes the tail by  $12.79 \text{ ms} \pm 12.41 \text{ ms}$  and by  $8.00 \text{ ms} \pm 13.12 \text{ ms}$  on average respectively (Figure 2E, bottom). Both fins also show a consistent difference in onset time of  $4.75 \text{ ms} \pm 13.69 \text{ ms}$  with regards to each other.

This promoted the question how fins coordinate with each other. We selected two example bout categories to represent the behavior categories of forward swimming (Slow 1) and turns (High Angle Turn) (Figure 2F). In order to investigate fin-fin coordination in time, we computed the rolling correlation between the fins (Figure 2G). Upon bout onset the fins are anti-correlated and move in anti-phase up to 20 ms before switching to a correlated moving in-phase pattern (Figure 2G). The timing of this transition depends on bout category with forward bouts switching earlier than turns.

The type of movement had a consistent influence on the temporal dynamics of fins with regards to each other. In order to examine if the type of movement also had an influence on the temporal co-fluctuation with the tail, we computed the correlation of ipsi- or contralateral fin with the tail. From previous studies we know that the 'trailing fin'/contralateral is more correlated with the tail [23]. The contralateral fin is more correlated with the tail across our chosen behavior categories, while the ipsilateral fin was anti-correlated for turns and escapes but not for forward swims (Figure 2H).

How do the fins go from moving in anti-phase to moving in-phase? This could be achieved in two ways. One option is that a temporal lag is introduced in the process. We computed the fin beat duration for two consecutive oscillations and found the leading fin/ipsilateral to have a shorter fin beat duration for the first oscillation cycle (Figure 2I, Figure S4D) as has been previously observed [23]. However this difference between fins disappears in the subsequent oscillation cycle as the fins begin to change from anti phase to moving in-phase. Another option is that the fins move at different frequencies. We computed instantaneous Beat Frequencies of Tail (TBF) and Fins (FBF). The ipsilateral fin has a higher FBF during the first 10 ms of the bout (Figure 2J). Notably, both fins reach their maximum beat frequency before the tail (Figure 2G). This frequency modulation could be the driver to switch from a synchronous pattern of oscillation to an alternating one that co-varies with the tail before the fin frequencies start to match over the time course of the bout.

Another parameter that seems to be modulated is the amplitudes of the fin movement with turns showing having a larger first fin abduction than forward swims (Figure 2C). However, in forward movements the amplitude for consecutive fin oscillations does not decrease to the same degree as for turns. In both types of movement, the contralateral fin exhibited a statistically higher amplitude for the first oscillation (Figure 2K), except for escape bouts which follow a 'tuck' pattern [37] (Figure S4C). Therefore fin movements are likely modulated across a range of features according to different types of tail movements in order to facilitate smooth and efficient swimming.

## Fin behavior can be mapped onto a low dimensional manifold that varies along fin features gradients

To gain a better idea as to what way fin movements can be modulated, we embedded them in a low dimensional space and examined how the dimensions co-varied with different bout features. We calculated an adjacency matrix based on the covariance between fin traces as a distance metric (Figure 4A). This is then used as a similarity matrix for spectral embedding (See methods 0.0.4).

Figure 3A shows the embedding along the three first eigenvectors colored along the gradient of each dimension. Figure 3B shows individual examples of fin movements along the 3 principal dimensions. Along each of the dimensions, a different feature is modulated, with fins along dimension 1 changing in amplitude (Figure 3B), fins in Dimension 3 change according to frequency (Figure 3B), while fins along dimension 2 change according to a nonlinear time vigor dependence (Figure 3B) in which fin movements with a high amplitude first oscillation lead to a time delay in the second oscillation and therefore subsequent oscillations.

Next, we asked what fin features describe the main gradients of variability obtained by the spectral embedding. To do so, we calculated the correlation between the principle axes of the embedding and various features of fin movements with a set of features such as amplitude, frequencies and number of oscillations extracted per bout (Figure 3C, Figure S6C, Table 1). As expected from the profiles of the uniformly sampled examples, the first dimension correlates with different features related to fin amplitude modulation, the third dimension captures temporal aspects such as frequency and number of oscillations, while the second dimension does not show strong correlation with these features as it seems to capture specific dependencies between them. Examples of maximum amplitude (computed as average between the two fins) for Dimension 1 and Frequency average of the two fins for Dimension 3 are shown on the gradient in Figure 3D and Figure 3E and more examples in Supplementary Figure S6. These features are consistent with the features modulated during bout onset dynamics.

Next, we wanted to see if bout categories - to which the embedding procedure is blind - can be found in this new representation. We compared three metrics to assess bout category stereotypy (See methods 0.0.5) within the manifold, which were euclidean distance either on the similarity matrix of the fins covariance, the embedding space or the geodesic distance on the embedding space (Figure 4B). Briefly, for each of these distances, we computed the ratio between the average distances of data points from the same bout category (inter-cluster) and distances of data points from different categories (intra-cluster). As the euclidean distance on the manifold had the lowest distance ratio we continued with it. To assess the best number of dimensions to describe we computed the distance ratio for up to 10 components with the metric and found this measure is stable after 3 components were chosen (Figure 4B). This consolidates the choice of the 3 first components of the embedding as they indeed de-

scribe the different features linked to fin movements. We found that many bout types are represented together in the 3-dimensional fin dynamics embedding, indicating that some bouts with close fin dynamics have also similar tail dynamics (Figure 4E). Different bout categories are accompanied by more or less consistent fin movements (see methods 0.0.4) (Figure 4D, Supplementary Figure S7). Here, for each bout category we computed the ratio between inter-cluster and intra-cluster average distances and categorized bout categories on an axis of stereotyped to non-stereotyped. Stereotyped movements were divided into three tiers based on the quantiles of the data. For Stereotyped bout types the fin dynamics are more consistent within a bout category than with dynamics outside of the category. These include Slow1, LLC, Spot Avoidance Turn and Burst Swim, whereas High Angle Turn, Approach Swim and Slow 2 are less stereotyped. This indicates that this category uses a larger variety of dynamics. Bout categories with little stereotyped fin dynamics include SLC, Routine Turn, J Turn and 0 Bend.

## Partially shared underlying dynamics between tail and fins

Lastly, we asked if fin dynamics can be generated from the same latent network as the tail dynamics. For this, we use the previously tail-only trained network from [33] (Figure 5A) to see whether the latent space dynamics of an RNN could also predict fin traces that it was previously blind to. In order to test this, we extracted latent variables  $z$  from the pre-trained network and employed a Ridge Regression to find the best mapping between  $z$  and fin time series using an 80/20 train-test split. For an unbiased analysis we used an equally sampled data set per bout category ( $n=200$ ). We used the trained Ridge Regression model to predict fin traces and used a sequence to sequence linear regression to assess the goodness of fit ( $R^2$ ) per for each sample (Examples per category are shown in Figure 5B, top row). The latent variables  $z$  carry enough information for a good prediction throughout most categories between 0.6 and 1.0, however the spread for some categories (Burst Swim, Long Latency C-Start) is larger (Figure 5B, bottom row).

We asked which features were responsible for a large

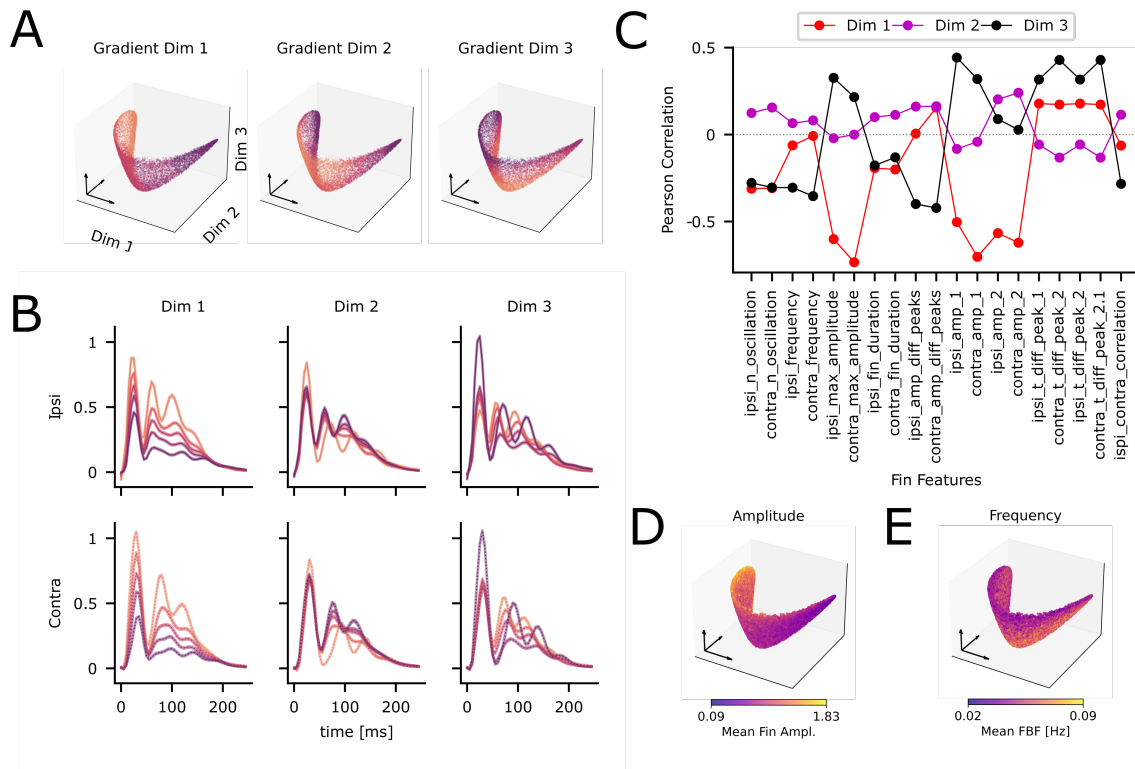


**Figure 3: Fin behavior can be mapped onto a low dimensional manifold that varies along fin features gradients.** (a) Embedding along the three first eigenvectors (3D view). Embedding colored by fins sampled uniformly along the Dimensions of the Embedding, Axes follow plot on left, (b) Mean traces along the samples of the Embedding for Ipsi- and Contralateral Fin, (c) Correlation between the principle axes of the embedding and various features of fin movements with a set of features from Table 1, (d) Embedding along the three first eigenvectors and colored by feature with maximum correlation for Dimension 1 (Mean First Amplitude of both Fins), (e) Embedding along the three first eigenvectors and colored by feature with maximum correlation for Dimension 3 (Mean Frequency of both Fins).

prediction error as these are features which are likely modulated differently from the tail. To investigate this, we focused on phase and power, two key characteristics of oscillatory signals. We performed a Fast Fourier Transform (FFT) and then selectively shuffled either phase or power. Using these altered signals, we reconstructed the time-domain signal and used it to predict fin traces. We observed a significant decrease in prediction accuracy for both modifications (Figure 5C), with phase shuffling affecting accuracy more than power shuffling. This suggests that the phase and relative timing of oscillatory waves are more critical for accurate predictions than the overall energy concentrated at specific frequencies. The reduction was dependent on bout category, with forward categories (Approach Swim, Slow1) having a large decrease while turns, e.g. Spot Avoidance Turns, were less affected (Figure 5C).

We have seen previously that features are modulated differentially between forward swims and turns. In order to investigate this further we looked at fin features previously described in table 1 and correlated these with the  $R^2$  of each bout. Fin peak vigor, fin number of oscillation and fin movement duration showed the strongest correlation regardless of category (Figure 5D). We saw

that specifically lower number of oscillations (Figure 5E) and lower fin peak amplitude seemed to affect the prediction of the network.  $R^2$ -Score mostly recapitulates dimension 1 of the fin manifold confirming that fin dynamics at the extreme end of amplitude are difficult to predict (Figure 5F). The network predicting success varies with fins that have these features irrespective of bout categories. However, certain bout categories might be more affected than others due to the fact that not all categories modulate all features in the same way and the degree of stereotypy.

## Discussion

Behavior is a complex and highly dimensional output of the nervous system. It needs to be adaptable and flexible but stereotyped enough for easy computations. For a simpler behavior description, reduced variability and easier interpretability, zebrafish larvae are often subjected to repeated stimuli while being restricted in their range of movements. While this has many advantages, some behaviors cannot be studied, especially coordination and motor pattern generation that rely on the unre-

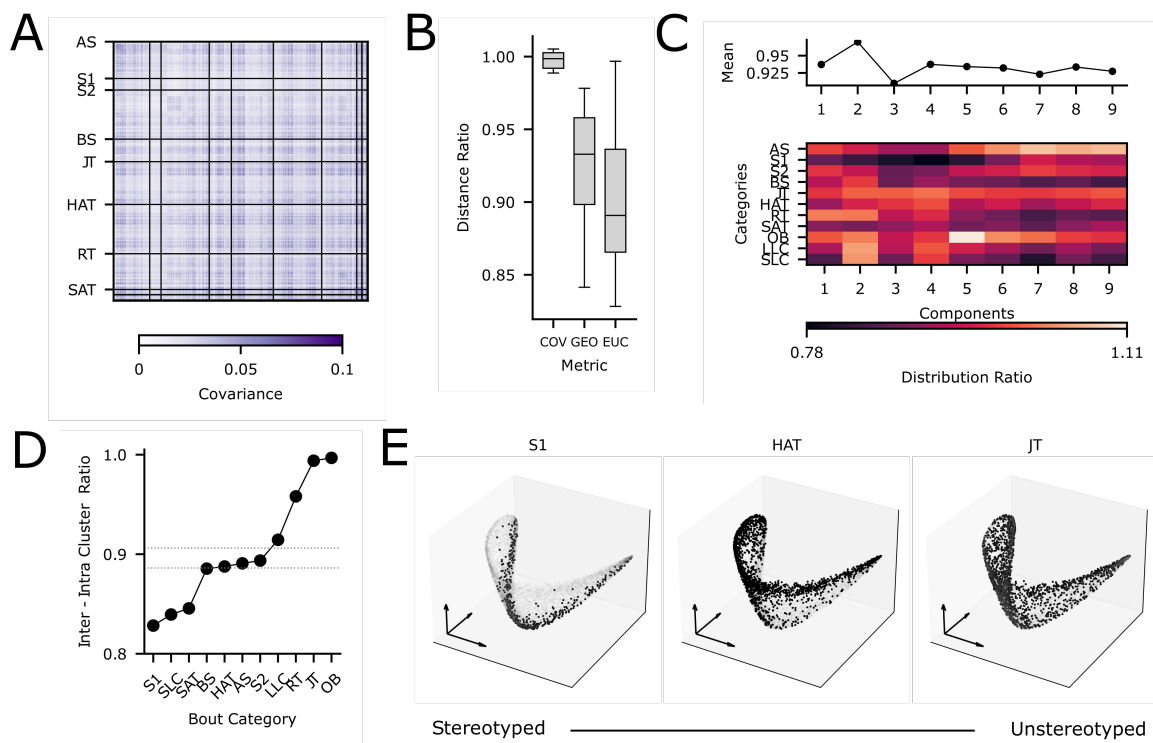


**Figure 4: Fin behavior can be mapped onto a low dimensional manifold that varies along fin features gradients.** (a) Covariance matrix of fin traces sorted by bout category, (b) Mean distance ratio between inter-cluster and intra-cluster bout categories for different metrics, COV: covariance distance, GEO: geodesic distance along the embedding and EUC: euclidean distance along the embedding, (c): The same ratio shown for EUC and its dependence on the numbers of components that are considered for the embedding. (D): Stereotypy of each bout type: the distance ratio computed separately for each bout category. (E): Examples of the distribution of data points along the embedding for 3 categories with different Stereotypy.



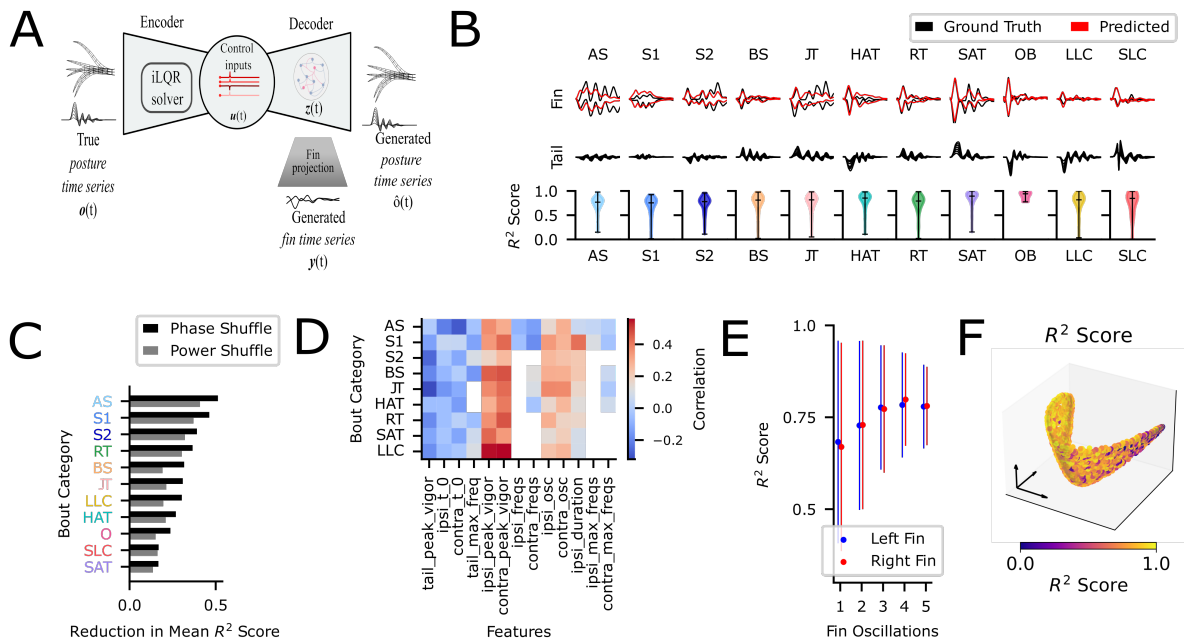


**Figure 5: Partially shared underlying dynamics between tail and fins.** (a) Input-driven dynamical system of tail kinematics share information of fin dynamics (iLQR-VAE Model) adapted from [33], (b) Examples of ground truth (black) and predicted (red) fin traces (top), tail trace for the examples (middle),  $R^2$  Score per bout category (bottom), (c) Reduction in Mean  $R^2$  Score for Phase and Power by Bout Category, (d) Feature Correlation of  $R^2$  Score with features from Table 1 per bout category, (e) Mean  $R^2$  Score by Number of Fin Oscillations, (f) Manifold colored by  $R^2$  Score.

stricted orchestration of multiple body parts. For this an unbiased and detailed description of natural behavior is key, in order to understand the pattern generation of motor circuits in vivo.

Here we aimed at providing such as detailed description to aid future interpretability of behavioral and neural data. For this we constructed a tracking rig to acquire high resolution data of all body parts of the fish with an automatic labeling and segmentation pipeline. We used a comprehensive bout type classification to have a smaller granularity of fish behavior without bias. Our embedding was able to give shed light on the principal axes used in movement generation of generate the rich and complex fin dynamics. Lastly, we show that a shared underlying network can generate both tail and fin movements, indicating a strong coupling.

## Improvement of Setup

We build a setup that follows a freely moving zebrafish larvae while imaging its behavior at 200 frames per second. This setup is akin to the setup presented in [12], however our presented setup has a higher frame rate (200 fps vs 60 fps) and a higher resolution enabling us to image the fins of the fish as dynamic coordinated processes with the tail. Previous tracking microscopy setups have already shown the possibilities also integrating neural imaging for the study of more naturalist hunter prey interactions and navigation [10, 11]. In order to capture more fine grained temporal dynamics we can im-

prove our raw behavioral data by using larger chip cameras with better frame rates and shorter exposures. To improve the quality of the motor tracking we could use model predictive control to allow for better recording of long continuous behavioral sequences.

Fish behavior in their natural environment is not restricted to one dimension in the horizontal plane and the fish also performs pitch, yaw and rolls. In order to investigate the other axis of movements, the full posture of the zebrafish should be studied in 3 dimensions. Other setups already enable 3D trajectory and posture reconstruction [38], but without the resolution necessary for fin tracking. 3D posture reconstruction requires a stereo views of the fish, which can be achieved using multiple cameras. Some fish, e.g. Rainbow trout, form complex fin shapes in 3D in order to initiate turning and breaking behaviors [39]. Furthermore, fins have been shown to play a role, specifically in lifting and diving [40, 41], making a characterization of fin movements incomplete without tracking fish in the horizontal axis.

Mapping data onto a skeletal model can help to study the biomechanics of movement in more depth, as already done in mice [42, 43]. Fin stiffness scales with propulsive forces in hydrodynamics studies of the bluegill sunfish [44]. Zebrafish larvae may not use their fins for propulsion or turning force generation, but the stiffness of their spine has direct implications of the head sway during development [45]. Therefore a mapping to a skeletal model might help us understand the biomechanics of movement generation better.

## Behavioral Categorization

The debate exists whether movements represent distinct behavioral categories or a smooth continuum of all possible behaviors. There is evidence of both in zebrafish. While some studies have shown multiple peaks in kinematic parameters showing categorical distinctions [46–50] up to the description of categories for tail and saccades [21, 51, 52], other studies described continuous variation in parameters, e.g. in prey capture [53, 54]. These two views are compatible as a range of intermediate movements exists in the movement landscapes.

Swimming speed lets us illustrate this. For forward locomotion at different swimming speeds, individual half beats lie on a continuum [55, 56], whereas at bout level the speed underlies discrete gaits [46, 50]. While gait differences are prominent in mice [57], *Drosophila* larvae and *C. Elegans* show continuity between behavioral states [58].

The question arises if the dynamics of the pectoral fins can be categorized. Previous studies proposed a categorization of fins into 'crawl' (alternating oscillations), 'tuck' (single abduction and following tucking of fins) and 'scream' (Munch's scream) [37] and investigated stereotyped fin dynamics associated with tail movements [23, 24]. Nonetheless, we saw that fin dynamics are modulated across multiple feature based axes that make a clear cut classification difficult, although not impossible. We acknowledge that our data captures a limited behavioral space during spontaneous swimming. To investigate this question further, we would need to construct a data set using an extensive library of stimuli as done for tail [21]. As for now we have investigated the principle features necessary to generate rich dynamics of the fins we see across movements.

Additionally, behavioral categorized can comprise more than a single body part. Combined behavioral motifs that comprise multiple body parts in 2D or 3D across multiple timescales can be seen in mice [17] and zebrafish [19]. In the future the investigation of the behavioral space of larval zebrafish should encompass all body parts as well as multiple contexts across timescales.

## Shared Underlying Dynamics

Applying the iLQL-VAE model to predict fin dynamics can give us potential insights on how motor commands are shared between body parts. We have seen that the model generalizes well with regards to fin dynamics as has been shown before on a *C. elegans* data set [33]. The prediction of fin dynamics without retraining suggests that latent variables underlying the generation of tail and fin movements share similarities and similar control strategies for both types of limb dynamics. Shared neuronal pathways that are used for overarching control, e.g. oscillatory patterns, could be reusable between behaviors and adaptive behavior could emerge due to perturbation of the input signals. However a shared control signal should be validated by electrophysiological recordings of both tail and fin motor neurons.

A possible caveat for the prediction and interpretation of the model is that the dimensionality of the model was reduced based on the tail. A reduction in perfor-

mance of the model with regards to fin dynamics could be attributed to the removal of features which are irrelevant to tail dynamics but important for fin dynamics. Fin movements also may be difficult to predict due to multiple reasons. First, fins do move in the horizontal as well as the vertical axis [39]. Second, fins have been implicated to play a role in postural control, which would require continuous control inputs rather than sparse ones. Lastly, the small sample size we used for equally sampling fins for all bout categories could lead to over fitting. A more comprehensive analysis should be repeated with a larger number of samples and by training different versions of the model with mixed data of fins and tail.

There is limited knowledge on how tail and fin movement generating circuits are connected and controlled on a neuronal level. Movement control inputs are sent by the Mesencephalic Locomotor Region (MLR) to spinal projection neurons (SPNs), which are conserved in vertebrates [59]. This happens via V2a neurons (*chx10+*) interneurons, which are necessary and sufficient for tail locomotor and rhythm generation [60–62], show tonic or phasic activity during swimming [63] and have an influence on duration and frequency [64]. Sub types of V2a interneurons control three muscle types and gait locomotion speeds [65]. These could potentially link the larger rhythm generating circuit with the fin circuit traced back to *dmrt3+* interneurons in the spinal cord [27]. Previous literature points towards that subsets of V0v and dI6 (*dmrt3+*) neurons receive input from V2a neurons directly in mice, where ablation of V2a neurons also altered left right coordination at intermediate to high frequencies making them a good target for shared network control [66]. However, so far no clear functional relationship between v2a and *dmrt3a+* neurons has been found in zebrafish [67]. Another potential connection could be both V3 and V0 neurons. V3 interneurons are implicated in left right coordination and gait stabilization in mice [68] and V0 are possibly responsible left right coordination and gait transitions as they are influenced by locomotion speed [69]. In zebrafish, ablation of commissary MCoD neurons (V0v neurons homologous) led to an increase in head jaw displacement during slow swimming [70] making them an interesting target to investigate for changes in both Tail-Fin and Fin-Fin coordination in the future. A confirmation of our prediction of a shared control network requires manipulation of the circuit at different levels to shed light on the overarching organization of command signals and the degree of shared information to instruct fins and tail.

## Conclusion

We have developed a robust behavioral tracking setup for the acquisition of high resolution behavior of zebrafish larvae including a pipeline for automatic labeling, segmentation and tail based classification. We have described stereotyped onset dynamics as well as identified a manifold of features in which fins can be embedded to generate all fin dynamics that we could observe. Lastly, we have shown that similar control inputs can predict both tail and fin movements, hinting at a shared underlying control. We hope this can provide insights into the generation of coordinated movements in larval zebrafish

and beyond.

## Author Contributions

K.K. and R.P. conceived the project. K.K. and N.v.B. developed the setups including tracking method, training of labeling pipeline. K.K. performed the experiments and developed the analysis pipeline. K.K., Y.F, O.P., T.M. performed data analysis and prepared figures. K.K. wrote the paper, with input from R.P and M.O.

## Acknowledgments

We thank the German Research Foundation (DFG) for support under Germany's Excellence Strategy within the framework of the Munich Cluster for Systems Neurology (EXC 2145 SyNergy, identifier 390857198) for funding R.P. Additionally, we acknowledge generous support from the Volkswagen Stiftung Life Initiative (VW-Grant; 5110828) to R.P. We would also like to thank the Portugues lab for insightful discussions and their input and encouragement.

## Materials and Methods

### Experimental Model and Subject Details

All animal experiments were done under approved procedures of the Technische Universität München and Regierung von Oberbayern. Zebrafish (*Danio rerio*) of TL strain were reared as adults at 27.5–28 °C under 14/10 day light cycle in a fish facility with full recirculation of water containing carbon-, bio-, and UV filter and 12% water change per day. pH of water was regulated at 7.0–7.5 with a 20 g/liter buffer and conductivity at 750–800 µS by the assistance of 100g/liter. Fish were kept in 3.5 liter tanks in groups of 10 to 17 animals and fed the adults twice a day with Gemma micron 300 (Skretting USA) and live food (artemia salina) and fed the larvae thrice a day with Sera micron Nature (Sera) and ST-1 (AquaSchwarz). All experiments were conducted on 5–7 dpf larvae, which still did not have determined sex. Over night, a male and a female or three males and three females were left in breeding in Sloping Breeding Tank or breeding tank (Tecniplast) a week before the experiment. The following day, eggs were collected in the morning, rinsed with facility water system water, and subsequently kept in batches of 20–40 in 90 cm Petri dishes with Danieau solution 0.3x (17.4 mM NaCl, 0.21 mM KCl, 0.12 mM MgSO<sub>4</sub>, 0.18 mM Ca(NO<sub>3</sub>)<sub>2</sub>, 1.5 mM HEPES, Sigma-Aldrich reagents) until hatching and in fish facility water thereafter. Larvae were incubated at 28.5°C and a 14/10 hour day/night cycle and the solution changed daily. The fish were maintained on a 14-10 light-dark cycle at 28 degree Celsius in groups of 20 larvae per 50 mm petri dish in fish water until the day of the experiment. Experiments were performed at room temperature (20 °C).

## Method Details

### 0.0.1 Setup Design

We built a high-speed 3D Setup using 2 linear stages (20 cm) and a z stage (range 7 mm) (PI Systems, custom build) that tracks the fish while its freely moving in the experimental arena (Figure 1A). The motor controller was connected to a computer with the following accessories (NI PCIe-6323, NI BNC-2110, NI SHC68-68-EPM with 1 m cable). The stages were mounted upside down onto a support structure from aluminum pillars and a bread-board (Thorlabs). A light-weight aluminum adapter was used to mount a camera (Ximea iQ, sensor size 1280 x 1024 px) with Objective (Edmund Optics, 35 mm f/1.65) with an IR filter (Thorlabs) to the z stage. Our setup has a pixel size of 70 px per mm. Below the stages a table cut from Plexiglas and Thorlabs mounts was holding the experimental arena for the fish. The experimental arena was constructed from a Plexiglas cut bottom and a curved Sylgard cutout arena with 50 mm diameter and 1 mm height with slanted edges. A 10 x 13 cm 45 degree cold mirror (Edmund Optics) allows for projection (ASUS P3E) of stimuli from below onto a semitransparent screen. The whole setup was put in a dark enclosure to minimize outside influence.

**Experimental design** Before the start of each experiment, the fish was placed in the experimental arena with a light background stimulus, and left to acclimatize for 5 to 10 minutes. This also included the motor tracking the fish, which was also meant to acclimatize the fish to the tracking procedure. Before the experiment starts, we run a spiral search to find the fish, which initiates the motors to follow a forward or backwards spiral adjusted to the size of the arena. This algorithm will also be triggered when the fish is lost during the experiment. For each experiment videos of 10 minutes of spontaneous swimming were acquired. After the completion of the experiment the fish was removed from the experimental arena. In this paper we have analyzed 97 experiments, containing 64 fish in total, and extracted 11063 bouts.

**Fish tracking** Data was acquired using Stytra [34]. Videos were acquired at 200 fps with an exposure time of 1 ms and saved alongside motor position logs and video timestamps. To identify the fish position in the image, we threshold the image and find the area with the highest value. For this area we calculated moments to check for size and shape constraints. If this area fits constraints it will be classified as eye 1 and removed from the image for the next steps. The image is cropped around eye 1 to speed up the algorithm. In a radius adjusted to pixel size (70 mm per px), the neighborhood is searched for other areas of similar size (labeled as eye 2). The midpoint between the eye 1 and eye 2 is set as tracking target representing the fishes head. The distance from middle of frame to the tracking target is converted to voltage and send to the motor controller to keep the fish head in the center of the image. The tracking algorithm has a run time of 0.9 ms.

**Image annotation and Fish pose Estimation** The acquired videos were processed using DeepLabCut [15]. The training set consisted of more than 1000 labeled frames with 14 key points on the fish body (Figure 1B): the anterior and posterior eye (left & right), the fish body (above the swim bladder), 5 points along the tail starting below the swim bladder and the fin base as well as tips (left & right). We split our data 80/20 in test and training set. We trained for 316,000 epochs and evaluated the performance after training based on the test loss, test pixel error and visual inspection. The test pixel error is close to the expected error in human labeling. We found the DeepLabCut trained network labeling of the eyes inaccurate, therefore we build a separate pipeline for eye annotation. From the DeepLabCut annotated data we identified mid eye key-points and a mid head key-point set between the former. For each identified eye midpoint we used a flood filling algorithm to grow an region of interest (ROI). Then, we computed the image moments of the ROI to identify its principle angle and vector length. The endpoints of the vector were labeled as anterior and posterior eye (left & right). The final eye angle is calculated as the angle between the body axis vector and the line perpendicular to the eye midpoint vector. Tail key-points were up-sampled to 10 segments.

We extract the fin and tail angles from the coordinates obtained through the labeling of the trained neural network. The Body axis vector was defined as the midpoint of the head and the body marker. Fin angles were defined as the angle between the vector from fin base to fin tip with regards to the body axis vector. Tail angles were computed between tail segments.

For this paper, we describe the fins as ipsilateral and contralateral fin, depending on the side of the first tail undulation, e.g. if the first tail undulation is left, the left fin is the ipsilateral fin and the right fin the contralateral fin.

**Tracking assessment** We assessed the tracking performance by looking at 4 indicators, namely the fraction of tracked frames, the tracking error, the length of tracking episodes and the mean length of spiral search episodes. First, we quantified the number of frames the fish was tracked per video. Tracked frames were defined as frames where the body key point of the trained network has a likelihood over 99%. Additionally, within the subset of tracked frames we quantified the number of tracked fin frames in which the fin markers for left and right fin were placed with above 95% likelihood by trained network. Second, we assessed the tracking error as a distance of the mid head key point to the middle of the image. We set the threshold at 2 mm (140 px) as this is the distance the head can take from the center while still preserving the full fish within the frame. We assumed a circular radius for simplicity. Third, we looked at the length of episodes and searching episodes in which the fish was not tracked to have statistics on how well our spiral search works.

**Temporal Segmentation of Bout Epochs** To segment bouts based on tail speed as well as to classify the tail into pre defined bout categories we used Megabouts[18]. These categories are Approach Swim, Slow1, Slow2, Burst Swim, J Turn, High Angle Turn,

Routine Turn, Spot Avoidance Turn, 0 Bend, Long Latency C-Start (LLC) and Short Latency C-Start (SLC). We dissected the data into 250 ms segments (bouts) for further processing. Bouts longer than this were ignored for analysis.

After extraction, we applied the following set of filter conditions to ensure good data quality for our extracted bouts. Firstly, we excluded bouts where the fish was closer than 1 mm to the border to ensure the movement was not influenced by the arena. Secondly, we ensured labeling quality and thresholded the data based on the DeepLabCut likelihood (above 99%) for the body marker. Lastly, we wanted to guarantee a good tail classification and used the Megabouts probability metric assigned to each bout when matching each bout class. We only considered bouts that during classification had a probability of more than 0.5. After the previous filtering steps, we manually excluded bouts with inaccurate segmentation. Only bouts after all these filtering steps were used for consecutive analysis.

**Fish trajectory reconstruction** Since the camera was moving with the fish, reconstruction of the trajectory was done by adding difference from center in the image for each fish position in x and y with the motor position in x and y. For the reconstruction we first filtered the position data of the motor. This was done by excluding motor distances moved under a manually defined threshold of 0.04 mm. This was done, because the motor performs small movements occurs during the motor settling on a specific point when the fish is static, thereby causing artifacts in the Reconstruction when the fish is static. These artifacts are negligible when the fish is moving.

## 0.0.2 Feature Extraction

**Peak-Valley Decomposition** For each bodypart (tail, ipsilateral/contralateral fin) we extracted local maxima and minima in the time series of angles in a bout-wise manner. We computed the average differential of the signal around each extrema (e.g., for a given maximum point, we averaged the differential respective to its two surrounding minima). A given extrema was only considered if this differential was larger than a manually-defined threshold based on inspection of the histogram of differentials (0.1 on the normalized angle trace). The full and half beats were calculated as the time difference between extrema (either peak-to-peak or peak-to-valley). The number of oscillations was calculated as the number of peaks above the manually defined threshold. Amplitudes of all peaks were extracted. The 'leading fin' was assigned as the fin, whose first peak occurs earlier in time.

## Tail- and Fin-Beat Frequencies (TBF and FBF)

Tail and Fin Beat Frequencies were approximated from the half-period of their oscillations. For every given bout, local minima and maxima for the tail and fin angle time-series were first identified. Instantaneous TBF and FBF were then computed as  $\frac{\Delta t^{-1}}{2}$ ,  $\Delta t$  corresponding to the elapsed time between a minimum and the following maximum (or viceversa). In order to avoid noise fluctuations



resulting in large frequency estimations, local extrema were only considered for TBF and FBF estimation if the signal changes around them were large enough. To determine this, we computed the average differential of the signal around each extrema (e.g., for a given maximum point, we averaged the differential respective to its two surrounding minima). A given extrema was only considered if this differential was larger than a manually-defined threshold (0.2 on the normalized angle trace).

**Rolling correlations** Rolling correlations between the two fin traces were computed by calculating the pairwise correlation of the two series using a 50 ms rolling window. A minimum of two time points was allowed for computation during initial and final segments of the time series, so that correlation estimations during the first and last 50 ms involve less time points.

### 0.0.3 Quantification and Statistical analysis

**Laterality index computations** The laterality index per fish was defined as follows:

$$\frac{n_L - n_R}{N} \quad (1)$$

This will give a result between -1 and 1. A positive value indicates that the fish has a bias towards leading more often with its left fin, a negative value means that the fish has a bias towards leading more often with its right fin. A result of 0 would indicate that the fish leads just as often with its left fin as its right fin.

### 0.0.4 Embedding and fin features mapping

To understand the distribution of fin movements we projected the fin traces into a lower dimensional space. A technique that insures preserving local distances is spectral embedding based on Laplacian Eigenmaps. We defined covariance between fin traces as a distance metric between fin movements. This allowed us to measure simultaneously temporal matching and vigor differences between fin traces as reported by amplitudes. The distances calculated from the covariance are constructed such that bouts with highly dependent fin traces are close to each other. The resulting adjacency matrix (Figure 3A) is then used then as a similarity matrix for spectral embedding. This embedding was intended to produce a low dimensional representation in which bouts with similar fin dynamics are also close in the new reduced space. The first step of the algorithm is to construct a weighted graph defined by its square  $N \times N$  symmetric weighted affinity matrix  $\mathbf{W} : \{\mathbf{w}_{ij}\}$ , with  $N$  number of bouts in the dataset. Here we considered a fully connected graph; i.e., the matrix  $\mathbf{W}$  is non-zero except on the diagonal, that is the graph does not contain any self-loops. We defined the weight between two nodes as:

$$w_{ij} = |\text{cov}(f_{ipsi}^i, f_{ipsi}^j)| + |\text{cov}(f_{cont}^i, f_{cont}^j)|, \quad (2)$$

where  $f_{ipsi}^i$  and  $f_{cont}^i$  are respectively the ipsilateral and contralateral fin traces from bout  $b_i$ . Therefore,

in this representation each bout is defined by an  $M$ -dimensional vector is the sum of timepoints in  $f_{ipsi}^i$  and  $f_{ipsi}^j$ . The purpose of the embedding is to have instead a low-dimensional representation in which each bout is defined by a  $k$ -dimensional vector  $c_i$  with  $k < M$  such as the weighted distances in the new representation are minimized:

$$\min_{\mathbf{c}} \sum_{i,j} w_{ij} \|c_i - c_j\|_2, \quad (3)$$

with  $\mathbf{c} = (c_1, c_2, \dots, c_N)^T$ . It turns out that the minimization problem in (3) is equivalent to minimizing  $\text{Tr}(\mathbf{c}^T \mathbf{L} \mathbf{c})$ , where  $\text{Tr}$  is the trace norm and  $\mathbf{L}$  is the graph Laplacian matrix. Finally, the new representation  $\mathbf{c}$  are called eigenmaps and are simply given by the eigenvectors corresponding to the  $k$  smallest non-zero eigenvalues [71].

### 0.0.5 Measures of stereotypy

In order to evaluate the stereotypy of bout categories along the fin dynamics, we used a ratio between inter-cluster and intra-cluster distances within a given representation of these dynamics. More precisely, one chooses first a given distance  $d$  between two fin traces  $i$  and  $j$ . The distances that we used are the covariance distance:

$$d_c(i, j) = 1 - w_{ij}, \quad (4)$$

with  $\{w_{ij}\}$  as in equation (2). The euclidean distance along the embedding that was defined as:

$$d_e(i, j) = \|c_i - c_j\|_2, \quad (5)$$

with  $c_i$  and  $c_j$  are the low dimensional representation vectors defined in (3). Finally, the geodesic distance along the embedding:

$$d_g(i, j) = \text{shortest\_path}_G[c_i, c_j], \quad (6)$$

the shortest path between points  $c_i$  and  $c_j$  on a graph  $G$  that we defined by taking the closest 4 nodes to each data point.

Once a distance is chosen, the distance ration for a given bout category  $\mathbf{b}$  is given as:

$$R_{\mathbf{b}} = \frac{\left\langle \sum_{i,j \in \mathbf{b}} d(i, j) \right\rangle}{\left\langle \sum_{\substack{i \in \mathbf{b} \\ j \notin \mathbf{b}}} d(i, j) \right\rangle}, \quad (7)$$

where the sign  $\langle \cdot \rangle$  means average over the number of pairs in the sum. This ratio was used to define stereotypy per bout category. Finally, the overall distance ratio that was used to evaluate the difference distance metrics is the ratio  $R = \langle R_{\mathbf{b}} \rangle$ : the average of the ratio defined in equation (7) over all the bout categories.

**Feature Correlation with Principal Axes** The features from Table 1 were computed bout-wise based on 0.0.2 and used to correlate the principal axes of the embedding. Here correlation values were computed between each feature vector  $\mathbf{x}_i$  and low-dimensional representation  $v_j$ .

**Table 1: Feature Descriptions**

Feature Name	Description
ipsi_n_oscillation	Number of oscillations on the ipsilateral side
contra_n_oscillation	Number of oscillations on the contralateral side
ipsi_frequency	Frequency of oscillations on the ipsilateral side
contra_frequency	Frequency of oscillations on the contralateral side
ipsi_max_amplitude	Maximum amplitude on the ipsilateral side
contra_max_amplitude	Maximum amplitude on the contralateral side
ipsi_fin_duration	Fin duration on the ipsilateral side
contra_fin_duration	Fin duration on the contralateral side
ipsi_amp_1	Amplitude of the first peak on the ipsilateral side
contra_amp_1	Amplitude of the first peak on the contralateral side
ipsi_amp_2	Amplitude of the second peak on the ipsilateral side
contra_amp_2	Amplitude of the second peak on the contralateral side
ipsi_amp_diff_peaks	Amplitude difference between first and second peak on the ipsilateral side
contra_amp_diff_peaks	Amplitude difference between first and second peak on the contralateral side
ipsi_t_diff_peak_1	Time difference between the first and second peak on the ipsilateral side
contra_t_diff_peak_1	Time difference between the first and second peak on the contralateral side
ipsi_t_diff_peak_2	Time difference between the second peak and third on the ipsilateral side
contra_t_diff_peak_2	Time difference between the second peak and third on the contralateral side
ispi_contra_correlation	Correlation between ipsilateral and contralateral fin time series

**Traces sampled in embedded space** For each axis, indices of bouts were sorted separately according to their value for each axis in the embedding. The sorted space was then split into 5 chunks for visualization purposes. Along each dimension the mean of all bouts in that chunk was plotted with standard deviation. This happened for ipsilateral and contralateral fin.

### 0.0.6 Model

To investigate if fin dynamics can be generated from the same latent network as the tail dynamics, we utilized a previously tail-only trained recurrent neural network (RNN) model published [33]. This model was originally developed to encapsulate the latent space dynamics of tail movements. We extracted latent variables from the pre-trained model and trained a Ridge Regression Model to find the best translation to fins with a 80-20 train-test split. For all these steps we used an equally sampled data set based on bout category (n=200). We assessed the prediction error ( $R^2$ ) using sequence-to-sequence linear regression to evaluate prediction accuracy across different fin movement categories. As a control we transformed the fins into Fourier space and then shuffled either the phase or the power spectrum (n=1000 shuffles). We then applied an inverse Fourier transform and assessed the prediction accuracy using the mean  $R^2$  for the ground truth fins per bout category and the shuffled controls respectively. Pearson correlation of  $R^2$  and features from Table 1 was performed to assess which fin variables influence the prediction accuracy.

### 0.0.7 Data and Software Availability

Code for data Processing and figure generation can be found [here](#). Sample and data is available upon request.

## References

1. Datta, S. R., Anderson, D. J., Branson, K., Perona, P. & Leifer, A. Computational Neuroethology: A Call to Action. en. *Neuron* **104**, 11–24. ISSN: 08966273 (Oct. 2019).

2. Anderson, D. J. & Perona, P. Toward a Science of Computational Ethology. en. *Neuron* **84**, 18–31. ISSN: 0896-6273 (Oct. 2014).
3. Maselli, A. et al. Beyond simple laboratory studies: Developing sophisticated models to study rich behavior. en. *Physics of Life Reviews* **46**, 220–244. ISSN: 15710645 (Sept. 2023).
4. Musall, S., Urai, A. E., Sussillo, D. & Churchland, A. K. Harnessing behavioral diversity to understand neural computations for cognition. en. *Current Opinion in Neurobiology* **58**, 229–238. ISSN: 09594388 (Oct. 2019).
5. Nastase, S. A., Goldstein, A. & Hasson, U. Keep it real: rethinking the primacy of experimental control in cognitive neuroscience. en. *NeuroImage* **222**, 117254. ISSN: 10538119 (Nov. 2020).
6. Musall, S., Kaufman, M. T., Juavinett, A. L., Gluf, S. & Churchland, A. K. Single-trial neural dynamics are dominated by richly varied movements. en. *Nature Neuroscience* **22**, 1677–1686. ISSN: 1097-6256, 1546-1726 (Oct. 2019).
7. Stringer, C. et al. Spontaneous behaviors drive multidimensional, brainwide activity. en. *Science* **364**, eaav7893. ISSN: 0036-8075, 1095-9203 (Apr. 2019).
8. Nguyen, J. et al. Whole-brain calcium imaging with cellular resolution in freely behaving *Caenorhabditis elegans*. *Proceedings of the National Academy of Sciences of the United States of America* **113**, E1074–E1081 (2016).
9. Venkatachalam, V. et al. Pan-neuronal imaging in roaming *Caenorhabditis elegans*. *Proceedings of the National Academy of Sciences of the United States of America* **113**, E1082–E1088 (2016).
10. Cong, L. et al. Rapid whole brain imaging of neural activity in freely behaving larval zebrafish (*Danio rerio*). en. *eLife* **6**, e28158. ISSN: 2050-084X (Sept. 2017).
11. Kim, D. H. et al. Pan-neuronal calcium imaging with cellular resolution in freely swimming zebrafish | *Nature Methods*. *Nature Methods* **14**, 1107–1114. ISSN: 1548-7105 (Nov. 2017).
12. Johnson, R. E. et al. Probabilistic Models of Larval Zebrafish Behavior Reveal Structure on Many Scales. en. *Current Biology* **30**, 70–82.e4. ISSN: 0960-9822 (Jan. 2020).
13. Symvoulidis, P. et al. NeuBTracker—imaging neurobehavioral dynamics in freely behaving fish. en. *Nature Methods* **14**, 1079–1082. ISSN: 1548-7091, 1548-7105 (Nov. 2017).
14. Nourizonoz, A. et al. EthoLoop: automated closed-loop neuroethology in naturalistic environments. en. *Nature Methods* **17**. Number: 10 Publisher: Nature Publishing Group, 1052–1059. ISSN: 1548-7105 (Oct. 2020).
15. Mathis, A. et al. DeepLabCut: markerless pose estimation of user-defined body parts with deep learning. en. *Nature Neuroscience* **21**, 1281–1289. ISSN: 1097-6256, 1546-1726 (Sept. 2018).
16. Wiltischko, A. et al. Mapping Sub-Second Structure in Mouse Behavior. en. *Neuron* **88**, 1121–1135. ISSN: 08966273 (Dec. 2015).
17. Weinreb, C. et al. Keypoint-MoSeq: parsing behavior by linking point tracking to pose dynamics. en. *Nature Methods* **21**, 1329–1339. ISSN: 1548-7091, 1548-7105 (July 2024).
18. Jouary, A. et al. Megabouts: a flexible pipeline for zebrafish locomotion analysis. en.
19. Mullen, P. N., Bowlby, B., Armstrong, H. C. & Zwart, M. F. PoseR - A deep learning toolbox for decoding animal behavior en. Apr. 2023.

20. Sridhar, G. *et al.* Uncovering multiscale structure in the variability of larval zebrafish navigation en. May 2024.
21. Marques, J. C., Lackner, S., Félix, R. & Orger, M. B. Structure of the Zebrafish Locomotor Repertoire Revealed with Unsupervised Behavioral Clustering. en. *Current Biology* **28**, 181–195.e5. ISSN: 0960-9822 (Jan. 2018).
22. Markov, D. A., Petrucco, L., Kist, A. M. & Portugues, R. A cerebellar internal model calibrates a feedback controller involved in sensorimotor control. en. *Nature Communications* **12**, 6694. ISSN: 2041-1723 (Nov. 2021).
23. Green, M. H., Ho, R. K. & Hale, M. E. Movement and function of the pectoral fins of the larval zebrafish (*Danio rerio*) during slow swimming. *Journal of Experimental Biology* **214**, 3111–3123. ISSN: 0022-0949 (Sept. 2011).
24. McClenahan, P., Troup, M. & Scott, E. K. Fin-Tail Coordination during Escape and Predatory Behavior in Larval Zebrafish. en. *PLoS ONE* **7** (ed Browman, H.) e32295. ISSN: 1932-6203 (Feb. 2012).
25. Grandel, H. & Schulte-Merker, S. The development of the paired fins in the Zebrafish (*Danio rerio*). en. *Mechanisms of Development* **79**, 99–120. ISSN: 09254773 (Dec. 1998).
26. Thorsen, D. H., Cassidy, J. J. & Hale, M. E. Swimming of larval zebrafish: fin-axis coordination and implications for function and neural control. *Journal of Experimental Biology* **207**, 4175–4183. ISSN: 0022-0949 (Nov. 2004).
27. Uemura, Y. *et al.* Neuronal Circuits That Control Rhythmic Pectoral Fin Movements in Zebrafish. en. *The Journal of Neuroscience* **40**, 6678–6690. ISSN: 0270-6474, 1529-2401 (Aug. 2020).
28. Bagnall, M. W. & McLean, D. L. Modular Organization of Axial Microcircuits in Zebrafish. en. *Science* **343**, 197–200. ISSN: 0036-8075, 1095-9203 (Jan. 2014).
29. Ampatzis, K., Song, J., Ausborn, J. & El Manira, A. Pattern of Innervation and Recruitment of Different Classes of Motoneurons in Adult Zebrafish. en. *Journal of Neuroscience* **33**, 10875–10886. ISSN: 0270-6474, 1529-2401 (June 2013).
30. Ampatzis, K., Song, J., Ausborn, J. & El Manira, A. Separate Microcircuit Modules of Distinct V2a Interneurons and Motoneurons Control the Speed of Locomotion. en. *Neuron* **83**, 934–943. ISSN: 08966273 (Aug. 2014).
31. Hale, M. E., Day, R. D., Thorsen, D. H. & Westneat, M. W. Pectoral fin coordination and gait transitions in steadily swimming juvenile reef fishes. en. *Journal of Experimental Biology* **209**, 3708–3718. ISSN: 1477-9145, 0022-0949 (Oct. 2006).
32. Eaton, R., Lee, R. & Foreman, M. The Mauthner cell and other identified neurons of the brainstem escape network of fish. en. *Progress in Neurobiology* **63**, 467–485. ISSN: 03010082 (Mar. 2001).
33. Mullen, T. S., Schimel, M., Hennequin, G., Machens, C. K. & Orger, M. B. Learning Interpretable Control Inputs and Dynamics underlying Animal Locomotion. en (2024).
34. Štih, V., Petrucco, L., Kist, A. M. & Portugues, R. Stytra: An open-source, integrated system for stimulation, tracking and closed-loop behavioral experiments. en. *PLoS Computational Biology* **15** (ed Battaglia, F. P.) e1006699. ISSN: 1553-7358 (Apr. 2019).
35. Huang, K.-H., Ahrens, M., Dunn, T. & Engert, F. Spinal Projection Neurons Control Turning Behaviors in Zebrafish. en. *Current Biology* **23**, 1566–1573. ISSN: 09609822 (Aug. 2013).
36. Horstick, E. J., Bayleyen, Y. & Burgess, H. A. Molecular and cellular determinants of motor asymmetry in zebrafish. en. *Nature Communications* **11**, 1170. ISSN: 2041-1723 (Mar. 2020).
37. Itoh, M. & Hatta, K. Munch's SCREAM: A spontaneous movement by zebrafish larvae featuring strong abduction of both pectoral fins often associated with a sudden bend. en. *Neuroscience Research* **94**, 17–27. ISSN: 01680102 (May 2015).
38. Ravan, A., Feng, R., Gruebele, M. & Chemla, Y. R. *Rapid automated 3-D pose estimation of larval zebrafish using a physical model-trained neural network* en. Pages: 2023.01.06.522821 Section: New Results. Jan. 2023.
39. Drucker, E. G. & Lauder, G. V. Function of pectoral fins in rainbow trout: behavioral repertoire and hydrodynamic forces. en. *Journal of Experimental Biology* **206**, 813–826. ISSN: 1477-9145, 0022-0949 (Mar. 2003).
40. Zhu, Y. *et al.* Scalable Apparatus to Measure Posture and Locomotion (SAMPL): a high-throughput solution to study unconstrained vertical behavior in small animals en. Pages: 2023.01.07.523102 Section: New Results. Jan. 2023.
41. Ehrlich, D. E. & Schoppik, D. A primal role for the vestibular sense in the development of coordinated locomotion. *eLife* **8** (eds Calabrese, R. L., Raymond, J. L., Raymond, J. L., McArthur, K. & Straka, H.) Publisher: eLife Sciences Publications, Ltd, e45839. ISSN: 2050-084X (Oct. 2019).
42. Monsees, A. *et al.* Estimation of skeletal kinematics in freely moving rodents. en. *Nature Methods* **19**. Number: 11 Publisher: Nature Publishing Group, 1500–1509. ISSN: 1548-7105 (Nov. 2022).
43. Dunn, T. W. *et al.* Geometric deep learning enables 3D kinematic profiling across species and environments. en. *Nature Methods* **18**. Number: 5 Publisher: Nature Publishing Group, 564–573. ISSN: 1548-7105 (May 2021).
44. Tangorra, J. L. *et al.* The effect of fin ray flexural rigidity on the propulsive forces generated by a biorobotic fish pectoral fin. en. *Journal of Experimental Biology* **213**, 4043–4054. ISSN: 1477-9145, 0022-0949 (Dec. 2010).
45. Danos, N. & Lauder, G. V. The ontogeny of fin function during routine turns in zebrafish *Danio rerio*. en. *Journal of Experimental Biology* **210**, 3374–3386. ISSN: 1477-9145, 0022-0949 (Oct. 2007).
46. Severi, K. *et al.* Neural Control and Modulation of Swimming Speed in the Larval Zebrafish. en. *Neuron* **83**, 692–707. ISSN: 08966273 (Aug. 2014).
47. Burgess, H. A. & Granato, M. Sensorimotor Gating in Larval Zebrafish. en. *The Journal of Neuroscience* **27**, 4984–4994. ISSN: 0270-6474, 1529-2401 (May 2007).
48. Borla, M. A., Palecek, B., Budick, S. & O'Malley, D. M. Prey Capture by Larval Zebrafish: Evidence for Fine Axial Motor Control. en. *Brain, Behavior and Evolution* **60**, 207–229. ISSN: 0006-8977, 1421-9743 (2002).
49. Burgess, H. A. & Granato, M. Modulation of locomotor activity in larval zebrafish during light adaptation. en. *Journal of Experimental Biology* **210**, 2526–2539. ISSN: 1477-9145, 0022-0949 (July 2007).
50. Budick, S. A. & O'Malley, D. M. Locomotor Repertoire of The Larval Zebrafish: Swimming, Turning and Prey Capture. en. *Journal of Experimental Biology* **203**, 2565–2579. ISSN: 0022-0949, 1477-9145 (Sept. 2000).
51. Dowell, C. K., Lau, J. Y., Antinucci, P. & Bianco, I. H. Kinetically distinct saccades are used in a context-dependent manner by larval zebrafish. en. *Current Biology* **34**, 4382–4396.e5. ISSN: 09609822 (Oct. 2024).
52. Dowell, C. K., Hawkins, T. & Bianco, I. H. Subsets of extraocular motoneurons produce kinematically distinct saccades during hunting and exploration. en. *Current Biology* **35**, 554–573.e6. ISSN: 09609822 (Feb. 2025).

53. Trivedi, C. A. & Bollmann, J. H. Visually driven chaining of elementary swim patterns into a goal-directed motor sequence: a virtual reality study of zebrafish prey capture. en. *Frontiers in Neural Circuits* **7**. ISSN: 1662-5110 (2013).
54. Patterson, B. W., Abraham, A. O., MacIver, M. A. & McLean, D. L. Visually guided gradation of prey capture movements in larval zebrafish. en. *Journal of Experimental Biology*, jeb.087742. ISSN: 1477-9145, 0022-0949 (Jan. 2013).
55. McLean, D. L., Masino, M. A., Koh, I. Y. Y., Lindquist, W. B. & Fetcho, J. R. Continuous shifts in the active set of spinal interneurons during changes in locomotor speed. en. *Nature Neuroscience* **11**, 1419–1429. ISSN: 1097-6256, 1546-1726 (Dec. 2008).
56. McLean, D. L., Fan, J., Higashijima, S.-i., Hale, M. E. & Fetcho, J. R. A topographic map of recruitment in spinal cord. en. *Nature* **446**, 71–75. ISSN: 0028-0836, 1476-4687 (Mar. 2007).
57. Bellardita, C. & Kiehn, O. Phenotypic Characterization of Speed-Associated Gait Changes in Mice Reveals Modular Organization of Locomotor Networks. en. *Current Biology* **25**, 1426–1436. ISSN: 09609822 (June 2015).
58. Szigeti, B., Deogade, A. & Webb, B. Searching for motifs in the behaviour of larval *Drosophila melanogaster* and *Caenorhabditis elegans* reveals continuity between behavioural states. en. *Journal of The Royal Society Interface* **12**, 20150899. ISSN: 1742-5689, 1742-5662 (Dec. 2015).
59. Grillner, S., Wallén, P., Saitoh, K., Kozlov, A. & Robertson, B. Neural bases of goal-directed locomotion in vertebrates—An overview. en. *Brain Research Reviews* **57**, 2–12. ISSN: 01650173 (Jan. 2008).
60. Kimura, Y., Okamura, Y. & Higashijima, S.-i. *alx*, a Zebrafish Homolog of *Chx10*, Marks Ipsilateral Descending Excitatory Interneurons That Participate in the Regulation of Spinal Locomotor Circuits. en. *The Journal of Neuroscience* **26**, 5684–5697. ISSN: 0270-6474, 1529-2401 (May 2006).
61. Ljunggren, E. E., Haupt, S., Ausborn, J., Ampatzis, K. & El Manira, A. Optogenetic Activation of Excitatory Premotor Interneurons Is Sufficient to Generate Coordinated Locomotor Activity in Larval Zebrafish. en. *The Journal of Neuroscience* **34**, 134–139. ISSN: 0270-6474, 1529-2401 (Jan. 2014).
62. Eklöf-Ljunggren, E. et al. Origin of excitation underlying locomotion in the spinal circuit of zebrafish. en. *Proceedings of the National Academy of Sciences* **109**, 5511–5516. ISSN: 0027-8424, 1091-6490 (Apr. 2012).
63. Kimura, Y. et al. Hindbrain V2a Neurons in the Excitation of Spinal Locomotor Circuits during Zebrafish Swimming. en. *Current Biology* **23**, 843–849. ISSN: 09609822 (May 2013).
64. Carbo-Tano, M. et al. The mesencephalic locomotor region recruits V2a reticulospinal neurons to drive forward locomotion in larval zebrafish. en. *Nature Neuroscience* **26**, 1775–1790. ISSN: 1097-6256, 1546-1726 (Oct. 2023).
65. Pallucchi, I. et al. Molecular blueprints for spinal circuit modules controlling locomotor speed in zebrafish. en. *Nature Neuroscience* **27**, 78–89. ISSN: 1097-6256, 1546-1726 (Jan. 2024).
66. Crone, S. A. et al. Genetic Ablation of V2a Ipsilateral Interneurons Disrupts Left-Right Locomotor Coordination in Mammalian Spinal Cord. en. *Neuron* **60**, 70–83. ISSN: 08966273 (Oct. 2008).
67. Bello-Rojas, S. *Development and Structure of Spinal Interneuron Connectivity in Larval Zebrafish* ProQuest Dissertations & Theses (Washington University in St. Louis, 2024).
68. Zhang, Y. et al. V3 Spinal Neurons Establish a Robust and Balanced Locomotor Rhythm during Walking. en. *Neuron* **60**, 84–96. ISSN: 08966273 (Oct. 2008).
69. Lanuza, G. M., Gosgnach, S., Pierani, A., Jessell, T. M. & Goulding, M. Genetic Identification of Spinal Interneurons that Coordinate Left-Right Locomotor Activity Necessary for Walking Movements. en. *Neuron* **42**, 375–386. ISSN: 08966273 (May 2004).
70. Kawano, K. et al. Long descending commissural V0v neurons ensure coordinated swimming movements along the body axis in larval zebrafish. en. *Scientific Reports* **12**, 4348. ISSN: 2045-2322 (Mar. 2022).
71. Belkin, M. & Niyogi, P. Laplacian Eigenmaps for Dimensionality Reduction and Data Representation. en. *Neural Computation* **15**, 1373–1396. ISSN: 0899-7667, 1530-888X (June 2003).



Supplementary figures

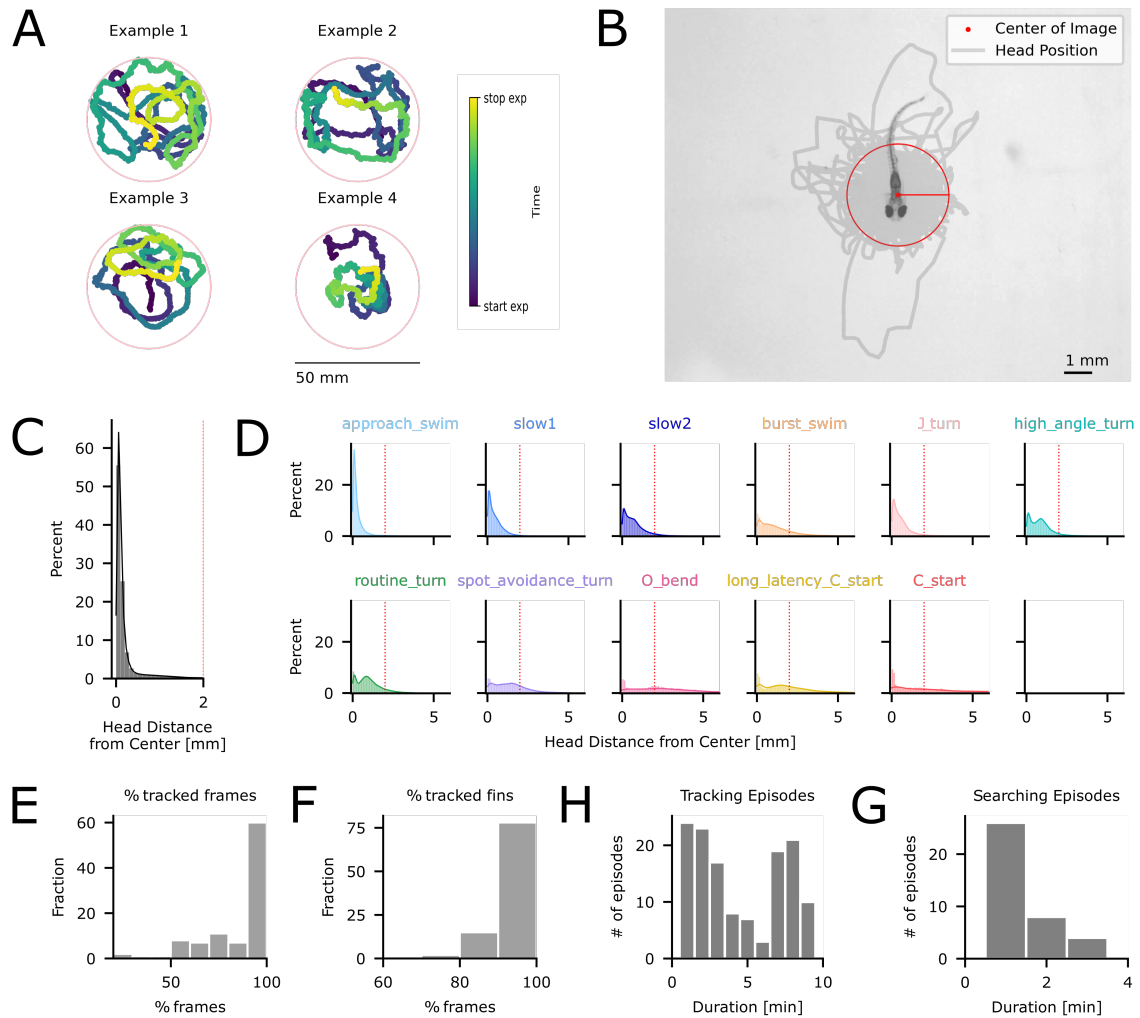


**Figure S1: Assessment of Tracking Performance.** (a) Four Example trajectories from experiment, (b) Example frame with the mid head position throughout the experiment overlaid in gray for the experiment, red circle denotes threshold for evaluating the pixel error, (c) Tracking error per bout for all bouts with threshold as red line, (d) Tracking error by bout categories with threshold as red line, (e) Fraction of tracked frames in percent, (f) Fraction of tracked fin frames in percent. This is a sub sample of tracked frames, (h) Duration of tracking episodes, (g) Duration of searching episodes.

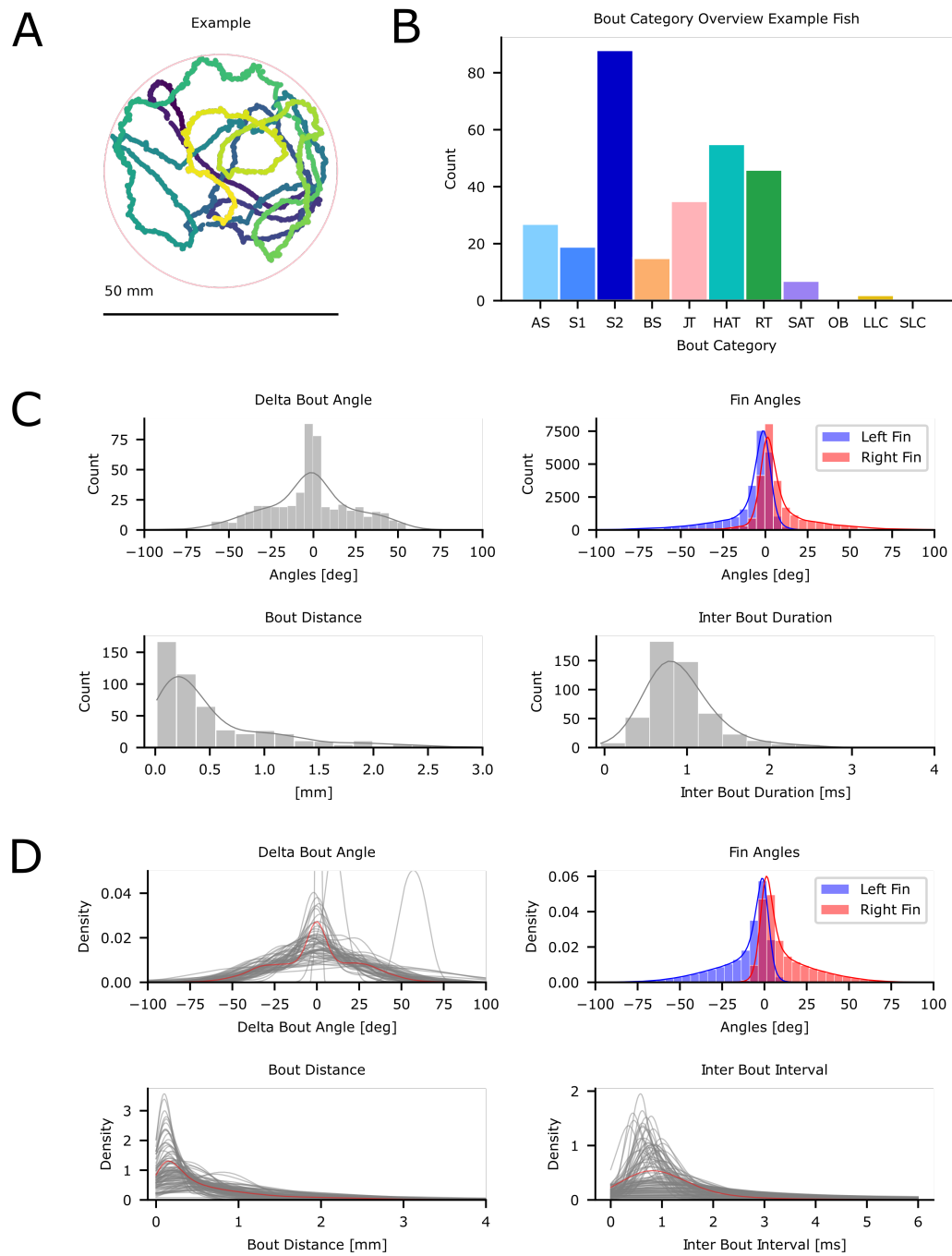


**Figure S2: Fish Behavioral Assessment.** (a) Trajectory of Example Fish, (b) Bout Categories for Example Fish, (c) Example Fish Bout Statistics: Delta Tail Angles (top left), left (blue) and right (red) Fin Angles (top right), Bout Distance (bottom left), Inter-Bout Interval (bottom right), (d) Pooled Bout Statistics: gray lines denote single fish, red line denotes mean across experiments. Delta Tail Angles (top left), left (blue) and right (red) Fin Angles (top right), Bout Distance (bottom left), Inter-Bout Interval (bottom right).

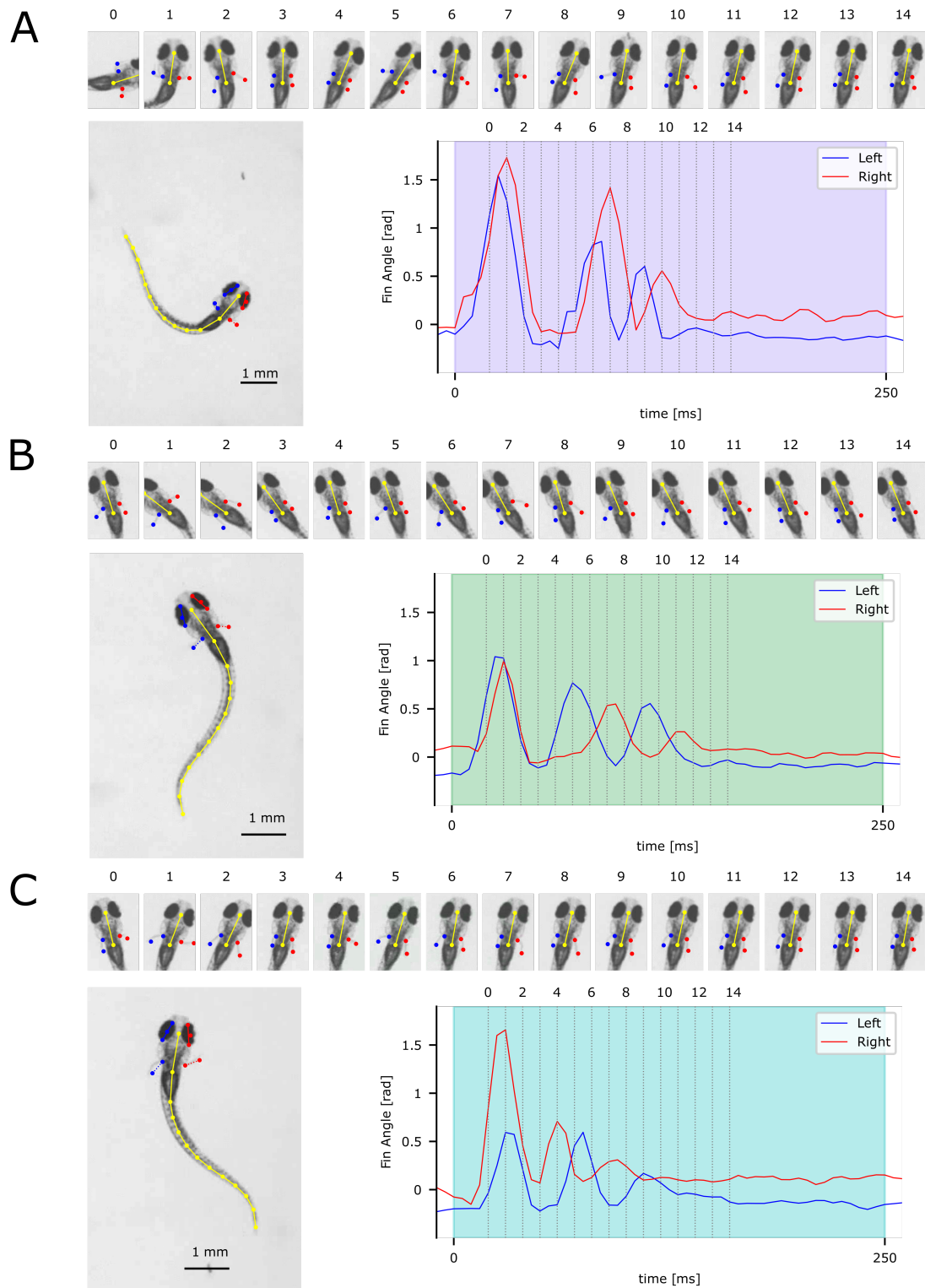


**Figure S3: Example Fin Traces with Images.** (a) Example of a *Spot Avoidance Turn*. (top) Example Frames from the Bout annotated with mid head and body key-points (yellow) as well as left (blue) and right (red) fin key-points. (bottom left) Bout Frame Overview between chosen frame 1 and 2. Fin Traces for the Bout (bottom right), (b) Example of a *Routine Turn*. Description follows (a). (c) Example of a *High Angle Turn*. Description follows (a).



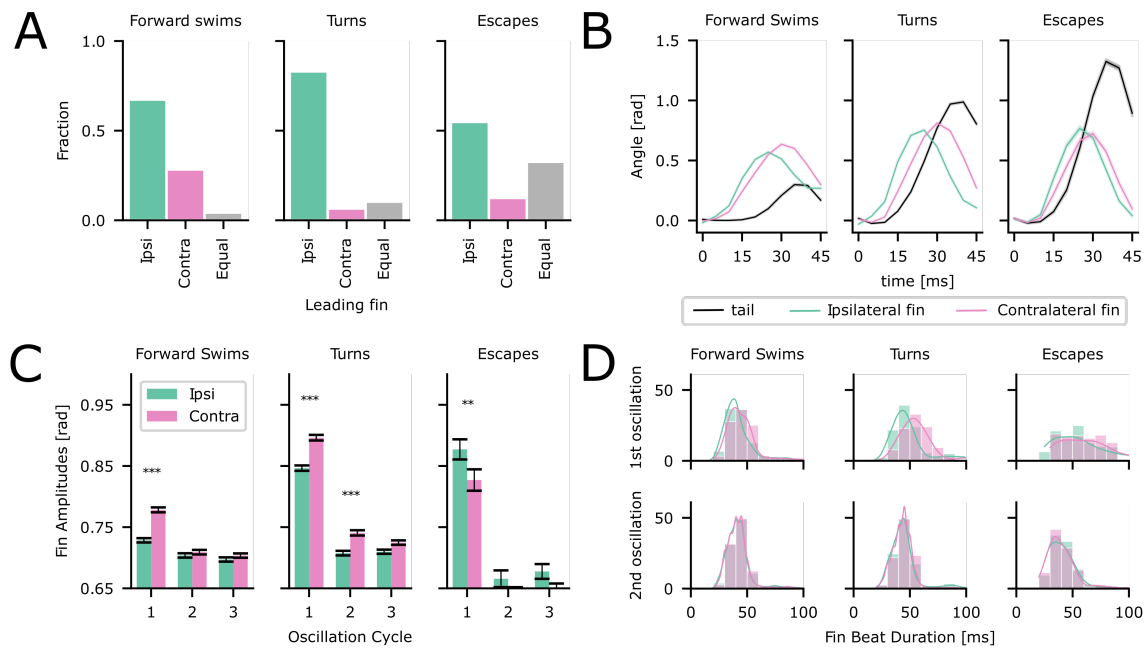


**Figure S4: Movement onsets across movement categories.** (a) Leading fin by movement categories, (b) Bout triggered average split by movement category. Mean traces with standard deviation plotted, (c) Amplitude of first fin abduction for ipsilateral and contralateral fin split by movement categories, (d) Fin Beat Duration across movement categories.

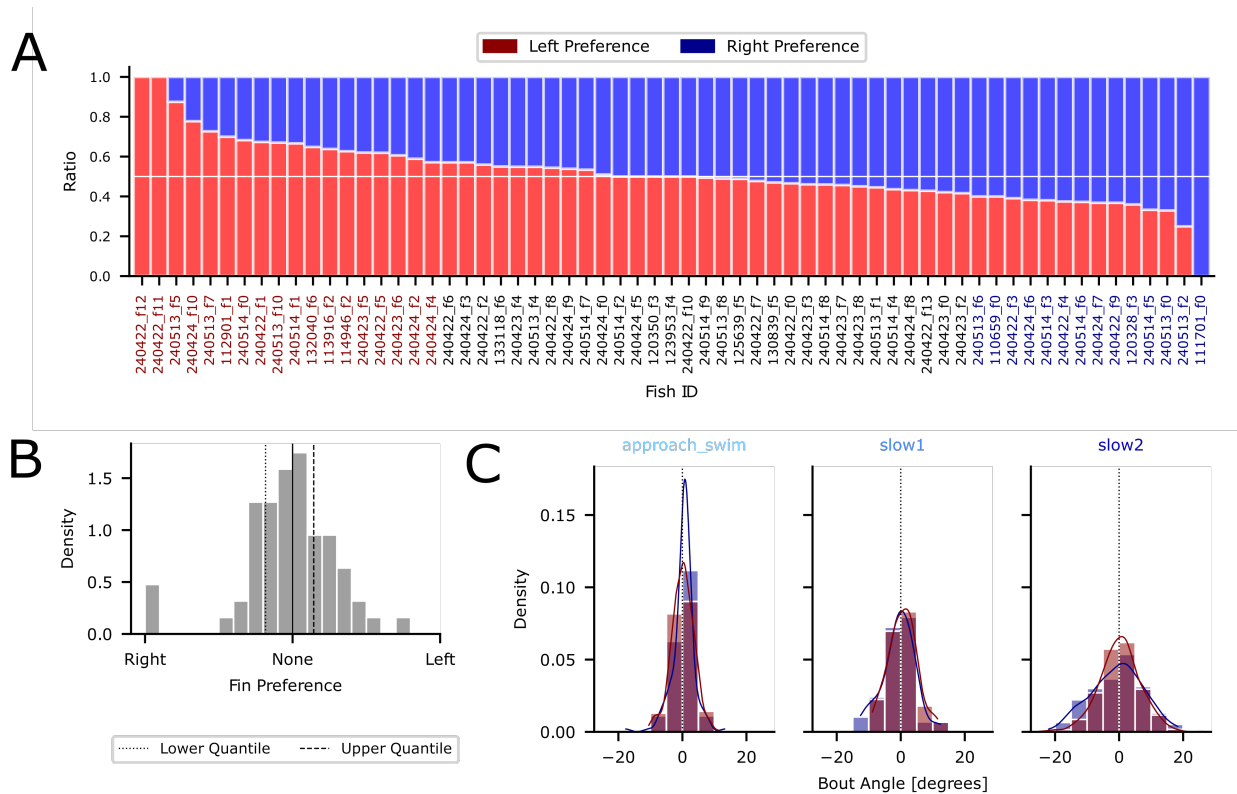


**Figure S5: Fin Bias.** (a) Ratio of fin usage (left (blue), right (red)) for forward swims for all fish. Biased Fish are annotated by ID color in either Left Preference (dark blue) or Right Preference (dark red), (b) Laterality score for all fish. Quantiles to classify fish as biased are plotted as dotted lines, (c) Delta Bout Angles for classified left or right biased fish for forward bout categories *Approach Swim*, *Slow 1*, *Slow 2*.

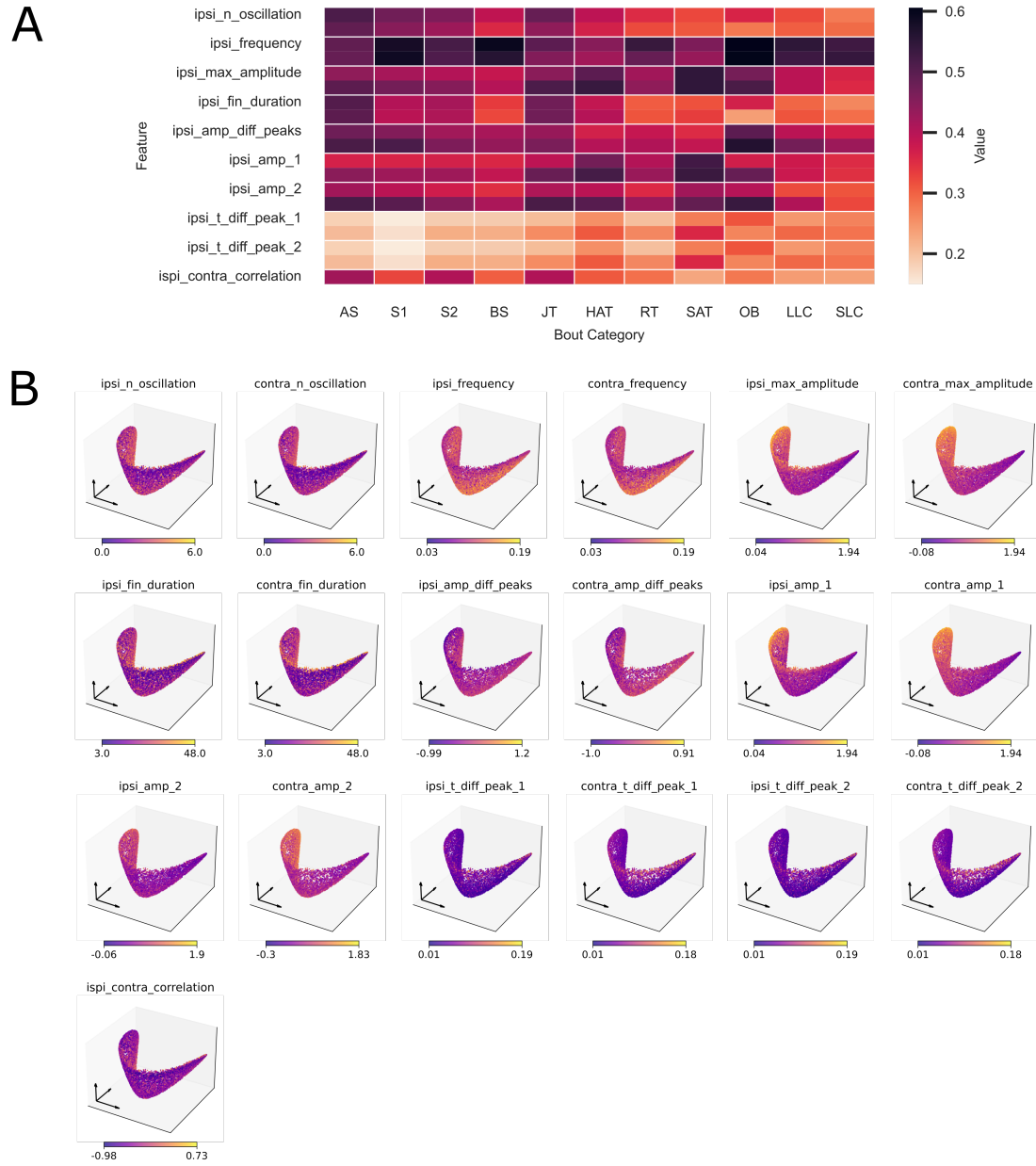


**Figure S6: Embedding colored by Fin Features.** (a) Heatmap of normalized features per bout category from Table 1, (b) Embedding colored by features from Table 1.

A

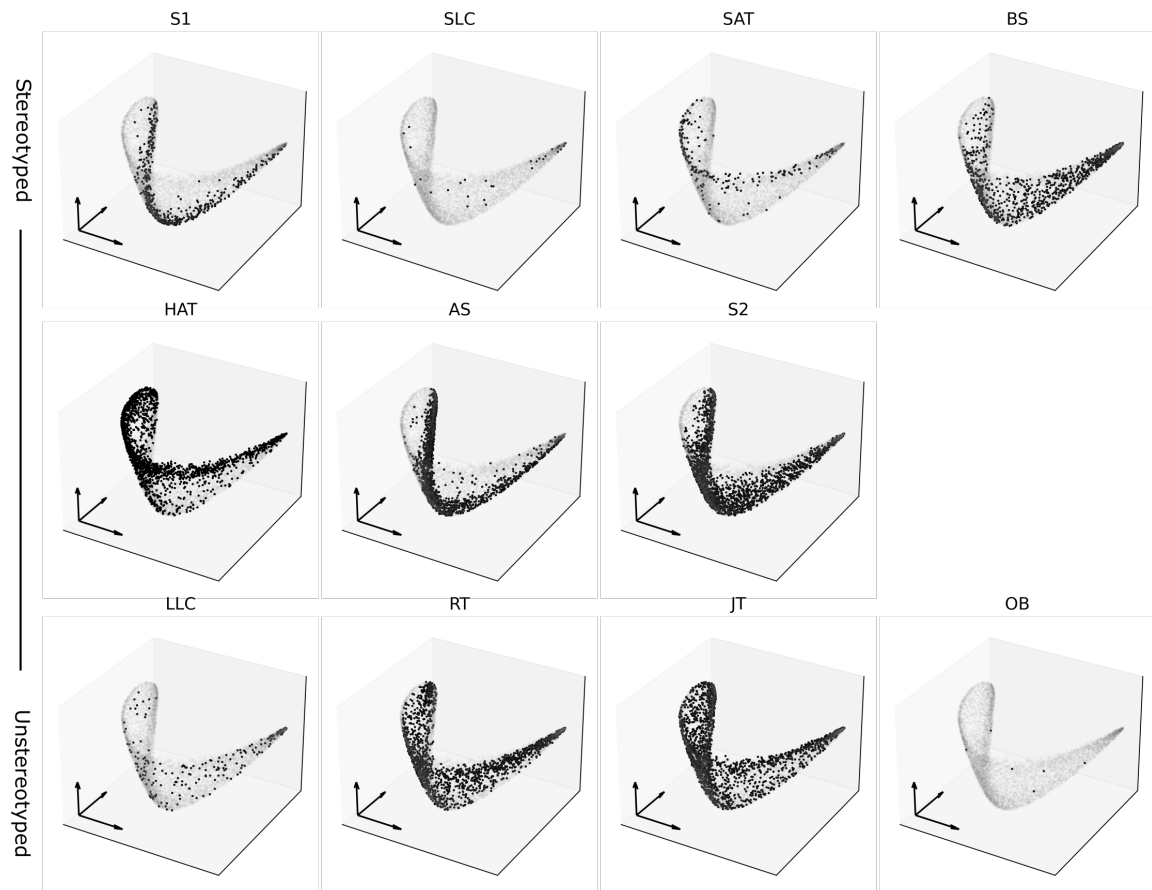


**Figure S7: Stereotyped Fin Movements.** (a) Embedding along the three first eigenvectors colored by bout category and ordered by stereotypy ratio value.